

UNIVERSITY OF HAWAII LIBRARY

VEHICLE HEALTH MONITORING SYSTEM USING MULTIPLE-MODEL
ADAPTIVE ESTIMATION

A THESIS SUBMITTED TO THE GRADUATE DIVISION OF THE
UNIVERSITY OF HAWAI'I IN PARTIAL FULFILLMENT
OF THE REQUIREMENTS FOR THE DEGREE OF

MASTER OF SCIENCE

IN

ELECTRICAL ENGINEERING

DECEMBER 2003

By
Xudong Wang

Thesis Committee:

Vassilis L. Syrmos, Chairperson
James Yee
Tep Dobry

Acknowledgements

I am deeply grateful to my advisor, Professor Vassilis L. Syrmos, for his enormous knowledge, patience, support, guidance and friendship throughout my M.S. program at University of Hawai'i. I would like to thank him for accepting me as his student and friend. I also want to thank Professor James Yee and Professor Tep Dobry for their so kindful help to my thesis work.

This work is dedicated to my parents for encourageing me always strive to be the best at everything I do. This work is also dedicated to my lovely wife, Min Zhong, whose endless support and encouragement are greatly appreciated; without her love, patience, support and sacrifices, I would not be where I am today.

I would like to thank my office mates, Martian Binonwangan, Mark Saewong, and Kaneshige Kenichi for their great encouragement and support.

Contents

Acknowledgements	iii
List of Tables	vi
List of Figures	vii
Abstract	1
1 Introduction	2
2 System model	8
2.1 Multiple-model representation	8
2.1.1 Basic Kalman filter equation	9
2.1.2 Noninteracting multiple-model estimator	11
2.1.3 Interacting multiple-model estimator	12
2.2 System failure modes	16
3 Fault-tolerant control system design	17
3.1 Multiple-hypothesis Kalman filter based FDI scheme	17
3.2 Interacting multiple-model estimator FDI algorithm	18
3.3 Reconfigurable controller design	21
3.3.1 Dynamic performance recovery-feedback controller design	22
3.3.2 Steady-state performance-recovery feedforward controller design	28
3.3.3 Reconfigurable control signal generation	30
4 Simulation results	31
4.1 System state-space equation description	31
4.1.1 DC motor	31
4.1.2 VTOL aircraft model	34
4.2 FDI performance evaluation of MH-KF and IMM algorithms	35
4.2.1 DC motor case	35
4.2.2 VTOL aircraft model case	42

4.3	Performance evaluation of FTCS for VTOL aircraft model based on IMM .	46
4.3.1	Eigenstructure and reconfigurable control gain	48
5	Conclusion	54
5.1	Discussions	54
5.2	Future work	55
	Bibliography	57

List of Tables

3.1	One cycle of multiple-hypothesis Kalman filter based FDI scheme	19
3.2	One cycle of interacting multiple-model based FDI scheme	20
3.3	Reconfigurable control signal generation scheme	30
4.1	DC motor model parameters	32
4.2	System Parameters description	33
4.3	Gyroscope and incremental encoder specification	34
4.4	VTOL aircraft model design parameters	45
4.5	System matrices for nominal and fault modes	45
4.6	Eigenvalues for nominal and fault modes	49
4.7	Eigenvectors of nominal and fault modes	49
4.8	Controller gains for fault-free and reconfigured systems	49
4.9	Values of quantitative performance indices	51
4.10	Ideal values of quantitative performance indices	51

List of Figures

1.1 Noninteracting multiple-model estimation algorithm	4
1.2 Interacting multiple-model estimation algorithm	5
1.3 General structure of IMM-based FDI and reconfigurable control scheme	7
3.1 Geometric interpretation of v_i, v_{i_A}	25
4.1 System model	34
4.2 Time Sequence	35
4.3 Failure sequence for DC motor	37
4.4 Log-likelihood function values of $MH - KF^I$ with $N = 20$	37
4.5 Log-likelihood function values of $MH - KF^{II}$ with $N = 20$	38
4.6 Log-likelihood function values of $MH - KF^I$ with $N = 40$	39
4.7 Log-likelihood function values of $MH - KF^{II}$ with $N = 40$	39
4.8 Posterior probabilities: $MH - KF^I$ with $MH - KF$ -based FDI scheme	40
4.9 Posterior probabilities: $MH - KF^{II}$ with $MH - KF$ -based FDI scheme	40
4.10 State transition diagram for $IMM - FDI^I$	41
4.11 State transition diagram for $IMM - FDI^{II}$	42
4.12 Posterior probabilities: $IMM - FDI^I$ with IMM -based FDI scheme	43
4.13 Posterior probabilities: $IMM - FDI^{II}$ with IMM -based FDI scheme	43
4.14 Estimation errors of Shaft angular velocity and angular position	44
4.15 Failure scenario of VTOL aircraft model	44
4.16 System dynamic response with state feedback	46
4.17 Log-likelihood function values for VTOL aircraft system modes with $N = 10$	47
4.18 IMM-based FDI simulation for VTOL aircraft system modes	47
4.19 State response under reconfigurable control	50
4.20 Mode transition probability under reconfigurable control	51
4.21 Output response z_1 under faults	52
4.22 Output response z_2 under faults	52
5.1 General structure of IMM-based FDI and reconfigurable control scheme with neural network	56

ABSTRACT

In this thesis, we propose two failure detection and identification (FDI) approaches based on the multiple-model estimation algorithm to monitor the health of vehicles, specifically aircraft applications. They detect and identify failing components of the vehicle, and the system variations. The dynamics of the vehicle are modeled as a stochastic hybrid system with uncertainty-unknown model structure or parameters. FDI performance is evaluated for each approach. We demonstrate the reliability, validity of these approaches by applying them to simulate aircraft machinery experiencing component failures or structural variations. The approaches that we surveyed are: (i) Multiple-Hypothesis Kalman Filter, and (ii) Interacting Multiple-Model (IMM) Estimator. By coupling the fault detection and identification (FDI) scheme with the reconfigurable controller design scheme, a fault-tolerant control system based on the multiple-model estimation algorithm is defined.

Chapter 1

Introduction

Modern engineering systems are becoming more and more sophisticated. Reliability, availability, and automatic supervision of technical processes and their control systems are important consideration in overall system design and operation. An integral element of a highly reliable, fault-tolerant control system (FTCS) is a control system that includes an efficient *fault detection and identification (FDI) scheme that can fast and reliably detect and isolate the sensor failures, actuator failures, and system component failures, and compensate and remedy the failures and prognosis the system to move from unscheduled maintenance to scheduled maintenance.*

A failure is defined to be any deviation of a system from its normal or intended behavior, diagnosis is the process of detecting an abnormality in the system behavior and isolating the cause or the source of this abnormality. Hard failure (i.e. complete mechanical breakdown) can be rapidly detected by on-line built-in-testing (BIT), and the more subtle or "soft" drifting-type failures can only be detected by the use of more sophisticated techniques, based on modern estimation/decision theory [1]. Many methods have been developed for fault detection and identification of dynamics systems over the last two decades [2, 3, 4, 5, 16, 17, 18], which can be categorized as: (i) confidence region overlap test, (ii) multiple-model based estimator, which can be categorized as noninteracting multiple-model based estimator and interacting multiple-model based estimator.

The confidence region overlap test was developed in [4, 5] to detect the fault in an inertial navigation system that was represented by a comprised dynamical model. The fault

decision criterion was based on the overlap test between two confidence region sheaths. One confidence region was about the expected nominal trajectory using a state propagator, while the other was using the Kalman filter state and covariance estimates. The overlap test was shown to result in a statistic scalar test that was compared to a pre-specified decision threshold in terms of the false alarming probability at any time instant to make failure/no failure decision. A more promising two-confidence region (CR2) failure detection algorithm was presented in [1]. Instead of iterating the set of the decision equations to calculate the test statistics, a geometric solution was developed to derive the decision, which led to lower computational burden and complexity of implementation.

Modern engineering systems are so sophisticated that systems subject to actuator, sensor failures and structural changes cannot be modeled well by a single set of equations of state that varies continuously. A more appropriate mathematical model for such a sophisticated system is the so-called stochastic hybrid system that consists of a set of possible system operation modes, which can be interpreted as the system mode set- θ . For the hybrid system, one of the most effective approaches for system health monitoring is based on the use of multiple models, which is called multiple-model based estimator. Multiple-model based estimator has been applied for the failure detection and identification for different engineering applications with different names, such as multiple-hypothesis test detector, and multiple-model adaptive estimator. Multiple-model based estimator involves the use of a bank of filters running in parallel, each based on the different hypothesis representing the underlying system behavior. Filters for corresponding failure modes are constructed, and the innovations from the various filters are used to compute the probability that the system is in that operation mode [3].

Multiple-hypothesis Kalman filter (MH-KF) is a noninteracting multiple-model estimation scheme. Each filter model can be characterized by a discrete state $\theta(t)$ from the set of all possible system modes, $\theta = \{\theta_1, \theta_2, \dots, \theta_M\}$. The multiple-hypothesis Kalman filter runs a bank of parallel filters, each based on a particular hypothesis matching to a possible system operation mode, and the pictorial hypothesis testing algorithm is shown in Figure 1.1. The Kalman filters are provided the measurement and the input, and produce state estimates and residuals. The residuals are used to compute conditional likelihood function values of the various hypotheses that are modeled in the Kalman filters, conditioned on the

history of the measurements received up to that time. Thus the failure/no failure decision is made and the system operation mode is identified. The hypothesis testing algorithm can also assign model-conditional probabilities to each of the hypotheses. Model-Conditional probabilities indicate the relative correctness of the filter models, and can be used to form a probability-weighted overall average state estimate (\hat{x}_{MMAE}). The multiple-hypothesis Kalman filter is applied for the FDI of “partial” and “total” sensor failures of DC motor.

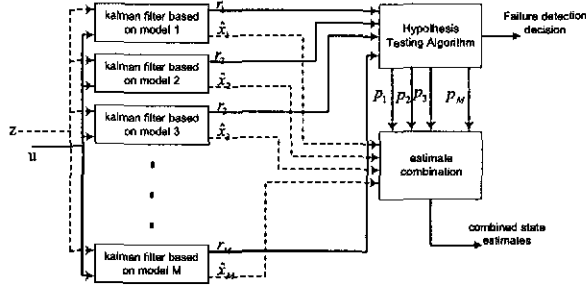


Figure 1.1: Noninteracting multiple-model estimation algorithm

As stated in [17], the multiple-model based FDI approaches are quite effective in handling problems with an unknown structure or parameters but without structural or parametric changes. In general, the system structure or parameter does change as component or subsystem failures. A lot of work has been done to compensate the weakness and to improve the performance of multiple-model based approaches, such as bounded conditional probabilities [10], removal of β dominance effect, Kalman filter retuning, probability smoothing, and increased residual propagation [13, 14].

By introducing the interaction between single-model-based filters into the FDI scheme, the interacting multiple-model (IMM) estimator in Figure 1.2 is a notable progress in the multiple-model estimation. It explicitly emulates the abrupt changes of the system by switching from one model to another in a probabilistic manner. The finite-state-machine technique is employed to represent the switching among various modes. The transition between the different models can be described as a first-order Markov process and is characterized by the transition probability matrix. IMM also consists of a bank of single-model-based filters running in parallel at each cycle. The initial state estimates at the beginning of each cycle for each filter are the mixture of all most recent estimates from the single-

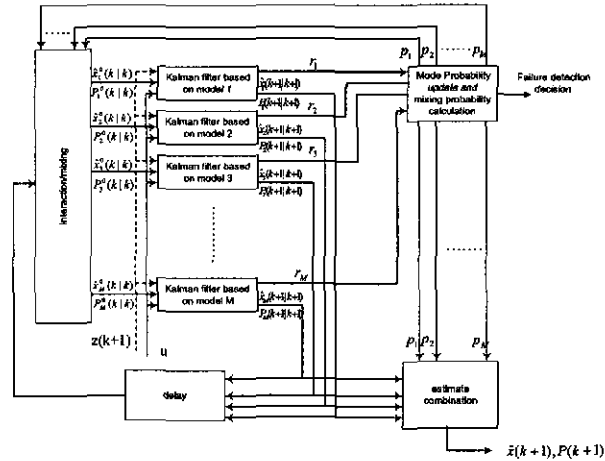


Figure 1.2: Interacting multiple-model estimation algorithm

model-based filters. It is the mixing that enables the IMM to effectively take into account the history of the mode without the exponential growth in computation and storage [9]. On the other hand, the posterior probabilities for each mode is calculated as the indicators of the mode in effect and mode transition at each decision time. Its main advantage over previous noninteracting multiple-model based FDI techniques is its reliability and quick detection and identification of simultaneous failures of sensors, actuators, and system component. In [16], IMM algorithm was used for the detection and identification of sensor and actuator failures in spacecraft autonomy. During this research, the effectiveness and superiority of interacting multiple-model estimation algorithm are demonstrated by the FDI performance of “partial” and “total” sensor failures of DC motor, and by the FDI performance of a longitudinal vertical takeoff and landing (VTOL) aircraft model.

The failures of sensors, actuators and system component will alter the characteristics of the system, such as stability, observability and controllability. It is necessary to apply the control laws to recover the system performance to the maximum extent, and meet the closed-loop design specification, such as dynamical response and steady-state performance. Based on the FDI results, it is applicable to design a fault-tolerant control to maintain the overall system stability and acceptable performance. In general, fault-tolerant control systems can be classified as passive and active. An active fault-tolerant control system compensates for faults either by selecting a precomputed control law or by synthesizing

a new control strategy on-line. The FDI schemes are used to detect and identify the failures and to activate control reconfiguration mechanisms. Typically, an active FTCS consists of three parts: a reconfigurable controller, an FDI schemes and a control law reconfiguration mechanism. Key issues is how to design: (1) a robust reconfigurable controller, (2) an FDI scheme with high sensitivity to failures and robustness to model uncertainties and external disturbances, and (3) a reconfiguration mechanism which can organize the reconfigurable controller in such a way that the prefault system performance can be recovered to the maximum extent.

In general, the existing active fault-tolerant control system design methods can be categorized based on the following approaches: linear quadratic regulator (LQR); eigenstructure assignment (EA); multiple models; adaptive control; pseudo inverse; and neural network. Among these methods, lots of research have been done on the multiple-model-based reconfigurable control. The approach developed in [10], known as multiple-model adaptive estimator/multiple-model adaptive control (MMAE/MMAC), uses LQR techniques to design the reconfigurable controllers and adaptively synthesize each of the controllers by use of maximum a posteriori probability (MAP). In this approach, the system under the presumed failure modes is represented by a set of models, and a bank of Kalman filters is used to estimate the states of the system based on the presumed failure modes. Innovation sequence of each Kalman filter is used to calculate the posterior probability, which can be interpreted as the failure/no failure indicator, and the overall system state estimates and the control inputs are the probability-weighted average of the signals from each model. However, the MMAE/MMAC is basically the non-interacting multiple-model estimation scheme. There is no interaction among Kalman filters. We already know the merits of the interacting multiple model estimation technique, it is very straightforward to extend the non-interacting MMAE/MMAC to interacting multiple-model adaptive estimator/multiple-model adaptive control. We can extend the proposed IMM-based FDI approach to the design of an integrated FDI and reconfigurable control. The IMM estimator is utilized to provide the FDI information, as well as the overall state estimates. The reconfiguration mechanism is based on the information from the mode posterior probability in the IMM algorithm. Since the stability and dynamic performance of the closed-loop system can be described by its eigenstructure, i.e., eigenvalues/eigenvectors, recovery of

the dynamic performance of the system subject to failures can be achieved via assigning the eigenstructure of the reconfigured system as close to that of the nominal system as possible. In this paper, LQR is used to design the control law for the nominal system, and EA is for the reconfigurable control laws of the impaired system. In addition, to achieve zero steady-state tracking even in the presence of faults, a set of feedforward control laws is also designed using an input weighting technique [11]. Figure 1.3 depicts the structure of the integrated IMM-based FDI and reconfigurable control.

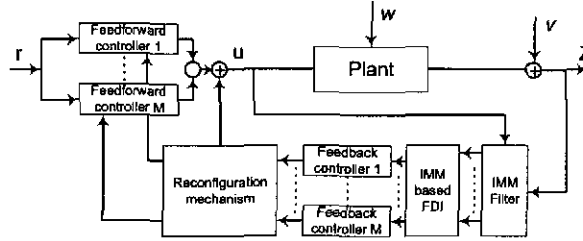


Figure 1.3: General structure of IMM-based FDI and reconfigurable control scheme

The remaining part of this paper is organized as follows: A description of a stochastic hybrid system and modeling of multiple failures are presented in the chapter 2. The FDI algorithm description and reconfigurable controller design scheme are in chapter 3. The performance evaluation of proposed FDI schemes and IMM-based fault-tolerant control system are presented and discussed in chapter 4. Finally, discussions and future work are given in chapter 5.

Chapter 2

System model

2.1 Multiple-model representation

The multiple-model estimation approach assumes that the actual system is adequately represented by a linear perturbation stochastic state model, with an uncertain (failure status) parameter vector affecting the matrices defining the structure of the model or depicting the statistics of the measurement or processing noises. Further the parameters are assumed to take on only discrete values to map the corresponding system models, and each system model is in certain probability drawn from a set of models designed to represent the all possible system behavior patterns. Then a Kalman filter is designed for each choice of system model, i.e., parameter value, which results in a bank of separate “elemental” filters. The stochastic hybrid systems are described as:

$$x(k+1) = A(k, \theta(k))x(k) + B(k, \theta(k))u(k) + w(k) \quad (2.1.1)$$

$$z(k+1) = H(k+1, \theta(k+1))x(k+1) + v(k+1) \quad (2.1.2)$$

where $x \in \mathbb{R}^n$ is the base state vector; $z \in \mathbb{R}^q$ is the (mode-dependent) measurement vector; $u \in \mathbb{R}^m$ is the control input vector; $w \in \mathbb{R}^n$ and $v \in \mathbb{R}^q$ are processing and measurement noises. $\theta(k)$ represents the current active system mode, and the set of all possible system modes is $\theta = (\theta_1, \theta_2, \dots, \theta_M)$.

The nonlinear system (2.1.1) is known as a “jump linear system”: It is linear given the system mode; however, the system may jump from one mode to another at a

random time. It can be observed from the system outputs that are in general noisy and mode-dependent. Therefore, the mode information is imbedded (i.e. not directly measured) in measurement sequences. It is applicable to filter the measurement sequence to determine which system mode is active, and thus get the health information of the system. According to the relationships among the Kalman filters and the methods of Kalman filter reinitialization, multiple-model estimator can be categorized as: noninteracting multiple-model; interacting multiple-model.

2.1.1 Basic Kalman filter equation

A LTI discrete-time system state space model associated with a particular hypothesized mode with the subscript j , i.e., the system mode is θ_j .

System dynamics

$$x_j(k+1) = A_j x_j(k) + B_j u(k) + w_j(k) \quad (2.1.3)$$

Sensor equation

$$z(k) = H_j x_j(k) + v_j(k) \quad (2.1.4)$$

where

x_j is the state vector,

A_j is the state transition matrix,

B_j is the control input matrix,

u is the known input,

w_j is an additive white Gaussian processing noise with zero mean and covariance

as:

$$E [w_j(m)w_j^T(n)] = Q_j \delta_{mn} \quad (2.1.5)$$

z is the measurement vector,

H_j is the measurement matrix,

v_j is an additive white Gaussian measurement noise with zero mean and covariance as:

$$E [v_j(m)v_j^T(n)] = R_j \delta_{mn} \quad (2.1.6)$$

The measurement noise sequence v_j and processing noise sequence w_j are independent of each other.

The Kalman filter algorithm uses the above LTI model to define time propagation and measurement update equations of the Kalman Filter state estimates and state estimation covariance matrix. The Kalman Filter state estimate propagation equation is:

$$\hat{x}_j(k+1|k) = A_j \hat{x}_j(k|k) + B_j u(k) \quad (2.1.7)$$

$$\hat{z}_j(k+1|k) = H_j \hat{x}_j(k+1|k) \quad (2.1.8)$$

where

$\hat{x}_j(k+1|k)$ is the state estimate before the measurement $z(k+1)$ is available,

$\hat{z}_j(k+1|k)$ is the estimate of the measurement before it becomes available, and

the state estimate covariance matrix propagation equation

$$P_j(k+1|k) = A_j P_j(k|k) A_j^T + Q_j \quad (2.1.9)$$

and when the measurement $z(k+1)$ is available, the state estimates are updated as:

$$\hat{x}_j(k+1|k+1) = \hat{x}_j(k+1|k) + K_j(k+1)(z(k+1) - H_j \hat{x}_j(k+1|k)) \quad (2.1.10)$$

where the Kalman filter gain is

$$K_j(k+1) = P_j(k+1|k) H_j^T [H_j P_j(k+1|k) H_j^T + R_j]^{-1} \quad (2.1.11)$$

The Kalman filter residual vector is defined as

$$r_j(k+1) = z(k+1) - H_j \hat{x}_j(k+1|k) \quad (2.1.12)$$

which is the difference between the measurements and the Kalman filter estimates. The residual vector can be assumed to be a set of independent zero-mean Gaussian random variable with covariance as:

$$\sigma_j^2(k+1) = H_j P_j(k+1|k) H_j^T + R_j \quad (2.1.13)$$

Finally, the Kalman filter state estimate covariance matrix is updated using

$$P_j(k+1|k+1) = P_j(k+1|k) - K_j(k+1) H_j P_j(k+1|k) \quad (2.1.14)$$

2.1.2 Noninteracting multiple-model estimator

Noninteracting multiple-model estimation approach defines a bank of Kalman filters running in parallel to represent all possible system modes. Each single-mode-based filter uses its own previous state estimates and filter covariance as the initial conditions at the current cycle, (2.1.15). There are no any interactions with each other.

$$\hat{x}_j^0(k|k) = \hat{x}_j(k|k) \quad (2.1.15)$$

$$P_j^0(k|k) = P_j(k|k) \quad (2.1.16)$$

where $\hat{x}_j^0(k|k)$, $P_j^0(k|k)$ are the initial conditions for j^{th} Kalman filter at time $k + 1$, and $\hat{x}_j(k|k)$, $P_j(k|k)$ are the state estimates and filter covariance of j^{th} Kalman filter at the k^{th} step.

Based upon the observed characteristics of the residuals $r_j(k)$ from each Kalman filter, the model-conditional probabilities are recursively evaluated, given the measurement history. This model-conditional probability can be an indicator of system status, compared with the prespecified threshold value. Since the Kalman filter residual is a white Gaussian sequence of zero mean and covariance as (2.1.13), we can get the model-conditional probability density function of the measurement, $z(k)$, at time k for the j^{th} hypothesis model, conditioned on the measurement history up to time $k - 1$, $Z(k - 1) = \{z(1), \dots, z(k - 1)\}$

$$f_{z(k)|\theta, Z(k-1)}(z|\theta_j, Z(k - 1)) = \beta \exp\{\cdot\} \quad j = 1, \dots, M \quad (2.1.17)$$

where

$$\beta = \frac{1}{(2\pi)^{\frac{q}{2}} |\sigma_j^2(k)|^{\frac{1}{2}}} \quad (2.1.18)$$

$$\{\cdot\} = \left\{ -\frac{1}{2} r_j^T(k) \sigma_j^{-2}(k) r_j(k) \right\} \quad (2.1.19)$$

We can define the conditional probability for a particular hypothesis model as:

$$p_j(k) = Pr(\theta = \theta_j | Z(k - 1)) \quad (2.1.20)$$

In [15], the conditional probability of j^{th} hypothesis model is updated as:

$$p_j(k) = \frac{f_{z(k)|\theta_j, Z(k-1)} p_j(k - 1)}{\sum_{i=1}^M f_{z(k)|\theta_i, Z(k-1)} p_i(k - 1)} \quad (2.1.21)$$

Here we use the prior conditional probabilities, $p_j(k - 1)$ to compute the conditional probabilities on the measurement at time k . For fault detection and identification problem, we can also use the conditional probabilities of the hypothesis models to detect the abnormality of the system.

$$p_j(k) = \max_i p_i(k) = \begin{cases} > p_T & \Rightarrow \theta_j : \text{mode } j \text{ occurred} \\ < p_T & \Rightarrow \theta_1 : \text{nominal mode occurred} \end{cases}$$

The conditional probabilities are used to compute the overall state estimates and covariance as:

$$\hat{x}_{MMAE}(k) = \sum_j \hat{x}_j(k) p_j(k) \quad (2.1.22)$$

$$P_{MMAE}(k) = \sum_j [P_j(k) + \tilde{x}_j(k) \tilde{x}_j(k)^T] p_j(k) \quad (2.1.23)$$

where $\hat{x}_j(k)$ and $P_j(k)$ are the j^{th} Kalman Filter state estimates and filter covariance, and

$$\tilde{x}_j(k) = \hat{x}_{MMAE}(k) - \hat{x}_j(k) \quad (2.1.24)$$

The noninteracting multiple-model algorithm is a recursive estimator:

- model-conditional reinitialization, each single-mode-based filter uses its own previous state estimates and filter covariance as the initial conditions at the current cycle
- model-conditional filtering
- model-conditional probability update based on the model-conditional prior probability and likelihood functions
- estimate combination, which yields overall state estimates and covariance

2.1.3 Interacting multiple-model estimator

The stochastic hybrid system (2.1.1) can be consider as a linear system with Markovian coefficients

$$x(k + 1) = A(\theta(k))x(k) + B(\theta(k))u(k) + w(k) \quad (2.1.25)$$

with observations

$$z(k) = C(\theta(k))x(k) + v(k) \quad (2.1.26)$$

where $\theta(k)$ is assumed to be a finite state Markov chain taking values in the discrete set $\theta = (\theta_1, \theta_2, \dots, \theta_M)$, i.e., the system mode sequence is an indirectly observable (or hidden) Markov chain [9].

Assume that the actual system is a discrete-time process, and then the Markov chain is a discrete-time-discrete-state (DSDT) Markov chain according to a transition probability matrix H_T :

$$H_T = \begin{pmatrix} \pi_{11} & \pi_{12} & \dots & \pi_{1M} \\ \pi_{21} & \pi_{22} & \dots & \pi_{2M} \\ \vdots & \vdots & \ddots & \vdots \\ \pi_{M1} & \pi_{M2} & \dots & \pi_{MM} \end{pmatrix}$$

where

$$\pi_{ij} = P[\theta(k+1) = \theta_j | \theta(k) = \theta_i] \quad \forall \quad \theta_i, \theta_j \in \theta \quad (2.1.27)$$

and

$$\sum_j \pi_{ij} = 1, \quad i = 1, 2, \dots, M \quad (2.1.28)$$

The transition probability matrix H_T is a design parameter.

The interaction among the Kalman filters can be described as the conditional probabilities mixing and evolution [9], depicted in Figure 1.2:

$$P[\theta(k)|Z(k)] \xrightarrow{\text{mixing}} P[\theta(k+1)|Z(k)] \quad (2.1.29)$$

$$P[x(k)|\theta(k), Z(k)] \xrightarrow{\text{mixing}} P[x(k)|\theta(k+1), Z(k)] \quad (2.1.30)$$

$$P[x(k)|\theta(k+1), Z(k)] \xrightarrow{\text{evolution}} P[x(k+1)|\theta(k+1), Z(k)] \quad (2.1.31)$$

$$P[\theta(k+1)|Z(k)] \xrightarrow{\text{Bayes}} P[\theta(k+1)|Z(k+1)] \quad (2.1.32)$$

$$P[x(k+1)|\theta(k+1), Z(k)] \xrightarrow{\text{Bayes}} P[x(k+1)|\theta(k+1), Z(k+1)] \quad (2.1.33)$$

For simplification, we define

$$\mu_j(k+1|k) = P[\theta(k+1) = \theta_j | Z(k)] \quad (2.1.34)$$

$$\mu_j(k+1) = P[\theta(k+1) = \theta_j | Z(k+1)] \quad (2.1.35)$$

The predicted mode probability (2.1.29) on the condition of $Z(k)$:

$$\mu_j(k+1|k) = P[\theta(k+1) = \theta_j | Z(k)] = \sum_i \pi_{ij} \mu_i(k) \quad (2.1.36)$$

which represents the prior probability for system mode θ_j .

In order to derive the representation of (2.1.30), we first introduce the following equation on the basis of the total probability:

$$P[x(k)|\theta(k+1) = \theta_j, Z(k)] = \sum_i P[x(k)|\theta(k) = \theta_i, Z(k)]P[\theta(k) = \theta_i|\theta(k+1) = \theta_j, Z(k)] \quad (2.1.37)$$

where

$$P[\theta(k) = \theta_i|\theta(k+1) = \theta_j, Z(k)] = \frac{\pi_{ij} \mu_i(k)}{\mu_j(k+1|k)} \quad (2.1.38)$$

The derivation of (2.1.31), (2.1.33) is directly from the iteration of Kalman filter. The residual sequence (2.1.12) is a zero mean Gaussian white noise sequence with covariance (2.1.13), and statistical hypothesis testing theory indicated that a good choice of likelihood function for failure detection would be in the form of conditional probability density, thus the likelihood function of j^{th} Kalman filter at time $k+1$ is:

$$L_j = \frac{1}{\sqrt{\det|2\pi\sigma_j^2|}} \exp\left(-\frac{r_j^T \sigma_j^{-2} r_j}{2}\right) \quad (2.1.39)$$

Thus (2.1.32) is the mode probability update:

$$\mu_j(k+1) = P[\theta(k+1) = \theta_j | Z(k+1)] = \frac{\mu_j(k+1|k)L_j}{\sum_i \mu_i(k+1|k)L_i} \quad (2.1.40)$$

On the basis of (2.1.30), the reinitialization of j^{th} Kalman filter can be described as:

$$\hat{x}_j^0(k|k) = E(x(k)|\theta(k+1) = \theta_j, Z(k)) \quad (2.1.41)$$

$$= \sum_i \frac{\hat{x}_i(k) \pi_{ij} \mu_i(k)}{\mu_j(k+1|k)} \quad (2.1.42)$$

$$P_j^0(k|k) = \text{cov}[\hat{x}_j^0(k|k)] \quad (2.1.43)$$

$$= \sum_i \frac{\pi_{ij} \mu_i(k) (P_i(k|k) + \tilde{x}_{ij}^0(k|k) \tilde{x}_{ij}^0(k|k)^T)}{\mu_j(k+1|k)} \quad (2.1.44)$$

where $\text{cov}[\cdot]$ stands for covariance and

$$\tilde{x}_{ij}^0(k|k) = \hat{x}_i^0(k|k) - \hat{x}_j(k|k) \quad (2.1.45)$$

From above equations, j^{th} filter at time $k+1$ has $\hat{x}_j^0(k|k)$ and $P_j^0(k|k)$ as its initial condition. This leads to the IMM estimator. The single-model-based filters clearly interact with each other.

For the output purpose, the overall state estimate and estimation error covariance are computed according to

$$\hat{x}(k+1) = \sum_j \hat{x}_j(k+1)\mu_j(k+1) \quad (2.1.46)$$

$$P(k+1) = \sum_j [P_i(k+1) + \tilde{x}_j(k+1)\tilde{x}_j(k+1)^T]\mu_j(k+1) \quad (2.1.47)$$

where

$$\tilde{x}_j(k+1) = \hat{x}(k+1) - \hat{x}_j(k+1) \quad (2.1.48)$$

Summarily, the IMM algorithm is a recursive estimator. In each cycle it consists of four major steps:

- model-conditional reinitialization (interacting or mixing of the estimates), in which the initial condition to the filter matched to a certain mode is obtained by mixing the estimates of all filters at the previous cycle;
- model-conditional filtering, based on the time update and measurement update of Kalman filter estimate
- model-conditional probability update, based on the model-conditional likelihood functions, and during this step, the system health decision (detecting the failure and identifying the failure mode) is determined by comparing the model-conditional posterior probability with the prespecified threshold
- estimate combination, which yields the overall state estimate as the probabilistically weighted sum of the updated state estimates of all filters. The probability of a mode being in effect plays a key role for determining the weights in the combination of state estimates and estimation error covariance.

2.2 System failure modes

In this research, system failure modes are focused on the A , B and C variations because they are the most common failure scenarios in the complex system. When we design the Kalman filter bank, we assumed that the Kalman filter model and the true model are of the same dimension and that the dynamics noise strength Q , measurement noise strength R are equivalent.

In the failure detection and identification of the aircraft flight control system, the actuator failure can be modelled as:

$$x(k+1) = Ax(k) + (B + \Delta B)u(k) + w(k) \quad (2.2.1)$$

where ΔB represents the fault-induced changes in actuators.

The system component failure can be represented as:

$$x(k+1) = (A + \Delta A)x(k) + Bu(k) + w(k) \quad (2.2.2)$$

For the sensor failure, we have two situations:

- **Partial sensor failure** Partial sensor failure can be modelled by increasing the measurement noise covariance matrix R
- **Total sensor failure** For the total sensor failure, a similar idea can be followed as (2.2.1), the failures can be modelled by annihilating the appropriate row of the measurement matrix H as:

$$z(k) = (H + \Delta H)x(k) + v(k) \quad (2.2.3)$$

Here we consider combination of the partial and total sensor failures, and simultaneous failures of the different sensors for DC motor FDI, and the combination of total sensor failure, actuator failure, and system component failure for VTOL aircraft model. These situations require that failure detection and identification algorithm to be more responsive and robust.

Chapter 3

Fault-tolerant control system design

For many applications, it is highly desirable to develop an aircraft flight control system with reconfigurable capabilities, which is able to detect and identify failures of sensors and /or actuators, even the system impairment, and then to recover the performance of the impaired system to the maximum extent. In general, an efficient FTCS consists of two parts: failure detection and identification scheme; reconfigurable control scheme. In this chapter, two main FDI scheme are developed on the basis of the algorithm in chapter 2: multiple-hypothesis Kalman filter; interacting multiple-model estimator. Linear quadratic regulator approach is used for reconfigurable feedback control law design of nominal system, while the eigenstructure assignment technique is for the impaired system.

3.1 Multiple-hypothesis Kalman filter based FDI scheme

The configuration of the multi-hypothesis Kalman filter failure detection method is shown in Figure 1.1. System observations are directly input into the bank of Kalman filters running in parallel. The number of Kalman filters depends on the number of modes that the system is expected to experience. Failure detection starts by monitoring the white Gaussian distributed residuals of each Kalman filter. The likelihood function value of each filter's residuals is calculated to determine the most probable mode—normal or failure—that has occurred given measurements. Essentially, the N most recent residual signals are examined to determine whether they differ significantly from the statistical description of their values that assumes no failures. The number N is a design parameter. A “sliding

“window” of the N most recent samples, with N on the order of 5 to 20, would be used. The log-likelihood function value is calculated as [6]

$$L_N = -0.5 \sum_{j=i-N+1}^i [r(j)^T \sigma^{-2} r(j) + \log |\sigma^2|] \quad (3.1.1)$$

Using (3.1.1), we calculate the likelihood value for each hypothesis model, and pick the maximum one which will represent the most possible operation status of the system. As we will see in chapter 4, there exists time delay for failure detection, and the delay depends on the size of the “sliding window”. On the other hand, as stated in chapter 2, we can calculate the mode-conditional probability, and compare it with the prespecified threshold value to make failure/no failure decision.

The algorithm of multiple-hypothesis Kalman filter can be summarized as Table 3.1

3.2 Interacting multiple-model estimator FDI algorithm

As described in chapter 2, the model-conditional probability is calculated, and can provide an indication of mode in effect at any time. It is natural to use it as an indication of a failure. By comparing with the threshold, the failure decision can be made at time k :

$$\mu_j(k) = \max_i \mu_i(k) = \begin{cases} > \mu_T & \rightarrow \theta_j : \text{mode } j \text{ occurred} \\ < \mu_T & \rightarrow \theta_1 : \text{nominal mode occurred} \end{cases}$$

Note that above failure decision rule provides not only the result of the failure detection but also the information of the type (sensor or actuator, system component), location (which sensor or actuator), size (total failure or partial failure with the fault magnitude) and fault occurrence time, that is, simultaneous detection and diagnosis. Taking into account the history of the modes enables the IMM algorithm to yield the best state estimation of the system subject to failures. Unlike the multiple-hypothesis Kalman filter, a “sliding window” is not necessary here to calculate likelihood function, which means that IMM algorithm can detect and identify failures almost in real-time.

The following Table 3.2 summarizes the interacting multiple-model FDI scheme.

Table 3.1: One cycle of multiple-hypothesis Kalman filter based FDI scheme

1. Model-conditional filter reinitialization (for $j = 1, \dots, M$):

$$\hat{x}_j^0(k|k) = \hat{x}_j(k|k), P_j^0(k|k) = P_j(k|k)$$

2. Model-conditional filter updating:

time update (from k to $k + 1$):

$$\hat{x}_j(k + 1|k) = A_j \hat{x}_j(k|k) + B_j u(k)$$

$$P_j(k + 1|k) = A_j P_j(k|k) A_j^T + Q_j$$

Kalman filter gain:

$$K_j(k + 1) = P_j(k + 1|k) H_j^T [H_j P_j(k + 1|k) H_j^T + R_j]^{-1}$$

Kalman filter measurement residual:

$$r_j(k + 1) = z(k + 1) - H_j \hat{x}_j(k + 1|k)$$

residual covariance:

$$\sigma_j^2(k + 1) = H_j P_j(k + 1|k) H_j^T + R_j$$

measurements update:

$$\hat{x}_j(k + 1|k + 1) = \hat{x}_j(k + 1|k) + K_j(k + 1) r_j(k + 1)$$

$$P_j(k + 1|k + 1) = P_j(k + 1|k) - K_j(k + 1) H_j P_j(k + 1|k)$$

3. Model-conditional probability update:

likelihood function:

$$L_j(k + 1) = \frac{1}{\sqrt{|2\pi\sigma_j^2(k+1)|}} \exp\left(-\frac{r_j^T(k+1)\sigma_j^{-2}(k+1)r_j(k+1)}{2}\right)$$

mode probability update:

$$p_j(k + 1) = \frac{p_j(k)L_j(k)}{\sum_i p_i(k)L_i(k)}$$

fault decision:

“sliding window” method:

$$L_{j,N}(k + 1) = \sum_{m=k-N+2}^{k+1} \log L_j(m)$$

$$\theta_j \text{ is the most possible system mode, } j = \arg \max_i L_{i,N}(k + 1)$$

conditional probability method:

$$\text{if } p_j(k + 1) = \max_i p_i(k + 1) > p_T \Rightarrow \theta_j$$

$$\text{if } p_j(k + 1) = \max_i p_i(k + 1) < p_T \Rightarrow \theta_1$$

4. Combination of state and covariance estimate:

overall state estimate:

$$\hat{x}_{MMAE}(k + 1) = \sum_j \hat{x}_j(k + 1) p_j(k + 1)$$

overall covariance estimate:

$$P_{MMAE}(k + 1) = \sum_j [P_j(k + 1) + \tilde{x}_j(k + 1) \tilde{x}_j^T(k + 1)]$$

$$\text{where } \tilde{x}_j(k + 1) = \hat{x}_{MMAE}(k + 1) - \hat{x}_j(k + 1)$$

Table 3.2: One cycle of interacting multiple-model based FDI scheme

1. Model-conditional filter reinitialization (for $j = 1, \dots, M$):

prior mode probability:

$$\mu_j(k+1|k) = \sum_i \pi_{ij} \mu_i(k)$$

mixing state estimate:

$$\hat{x}_j^0(k|k) = \sum_i \frac{\hat{x}_i(k) \pi_{ij} \mu_i(k)}{\mu_j(k+1|k)}$$

mixing covariance:

$$P_j^0(k|k) = \sum_i \frac{\pi_{ij} \mu_i(k) (P_i(k|k) + \tilde{x}_{ij}^0(k|k) \tilde{x}_{ij}^0(k|k)^T)}{\mu_j(k+1|k)}$$

$$\text{where } \tilde{x}_{ij}^0(k|k) = \hat{x}_i^0(k|k) - \hat{x}_j(k|k)$$

2. Model-conditional filter updating:

time update (from k to $k+1$):

$$\hat{x}_j(k+1|k) = A_j \hat{x}_j(k|k) + B_j u(k)$$

$$P_j(k+1|k) = A_j P_j(k|k) A_j^T + Q_j$$

Kalman filter gain:

$$K_j(k+1) = P_j(k+1|k) H_j^T [H_j P_j(k+1|k) H_j^T + R_j]^{-1}$$

Kalman filter measurement residual:

$$r_j(k+1) = z(k+1) - H_j \hat{x}_j(k+1|k)$$

residual covariance:

$$\sigma_j^2(k+1) = H_j P_j(k+1|k) H_j^T + R_j$$

measurements update:

$$\hat{x}_j(k+1|k+1) = \hat{x}_j(k+1|k) + K_j(k+1) r_j(k+1)$$

$$P_j(k+1|k+1) = P_j(k+1|k) - K_j(k+1) H_j P_j(k+1|k)$$

3. Model-conditional probability update:

likelihood function:

$$L_j(k+1) = \frac{1}{\sqrt{|2\pi\sigma_j^2(k+1)|}} \exp\left(-\frac{r_j^T(k+1)\sigma_j^{-2}(k+1)r_j(k+1)}{2}\right)$$

mode probability update:

$$\mu_j(k+1) = \frac{\mu_j(k+1|k) L_j(k+1)}{\sum_i \mu_i(k+1|k) L_i(k+1)}$$

fault decision:

$$\text{if } \mu_j(k+1) = \max_i \mu_i(k+1) > \mu_T \Rightarrow \theta_j$$

$$\text{if } \mu_j(k+1) = \max_i \mu_i(k+1) < \mu_T \Rightarrow \theta_1$$

4. Combination of state and covariance estimate:

overall state estimate:

$$\hat{x}(k+1) = \sum_j \hat{x}_j(k+1) \mu_j(k+1)$$

overall covariance estimate:

$$P(k+1) = \sum_j [P_j(k+1) + \tilde{x}_j(k+1) \tilde{x}_j(k+1)^T]$$

$$\text{where } \tilde{x}_j(k+1) = \hat{x}(k+1) - \hat{x}_j(k+1)$$

3.3 Reconfigurable controller design

In order to detect and identify failures of the sensors, actuators, and system components, the system must be asymptotically stable. Faster state convergence rate is, the better failure detection and identification performance we will get. In [12], lots of researches have been done on using LQR to design the optimal control to stabilize the system dynamic performance. EA method is used to recover the dynamic performance of impaired systems to the maximum extent. The reason for the choice of EA for impaired systems is that when the performance specifications are given in terms of system eigenstructure, the eigenstructure can be achieved exactly for the stability and desired dynamic performance. The extent of performance recovery highly depends on the number of actuators and measurements available. In general, the LQR-based control design will guarantee the closed-loop system stability and certain degree of robustness. For the above reason, the EA is used for the design of reconfigurable controller while LQR is for the design of the nominal controller. To achieve steady-state tracking, reconfigurable feedforward controllers are also synthesized using input weighting approach. The DC motor system and VOTL aircraft control system are both multiple inputs and multiple outputs (MIMO) system.

The main results of eigenstructure assignment by state feedback and output feedback are given in the following theorems [7].

Theorem 1 *For a dynamic system described in (2.1.1) with a full state feedback given by*

$$u(k) = Kx(k) + Gr(k) \quad (3.3.1)$$

there exists a matrix gain $K \in \mathbb{R}^{m \times n}$ such that

1. *n self-conjugate eigenvalues can be assigned arbitrarily*
2. *r entries in each corresponding eigenvector of a total of n eigenvectors can be arbitrarily selected*
3. *the achievable eigenvectors must lie in the subspace spanned by $\{(\lambda_i I - A)^{-1}B, i = 1, \dots, n\}$*

where λ_i is the i^{th} closed-loop eigenvalues of the closed-loop system, $G \in \mathbb{R}^{m \times m}$ is the input weighting matrix of the closed-loop system, and $r(k)$ is the external input to the closed-loop system.

In situations where only the output feedback is available, the results of eigenstructure assignment can be stated as:

Theorem 2 For a dynamic system described in (2.1.1) with an output feedback given by

$$u(k) = Kz(k) + Gr(k) \quad (3.3.2)$$

there exists a matrix gain $K \in \mathbb{R}^{m \times q}$ such that

1. $\max(m, q)$ self-conjugate eigenvalues can be assigned arbitrarily
2. $\max(m, q)$ eigenvectors can be partially assigned with $\min(m, q)$ entries in each vector arbitrarily chosen
3. the achievable eigenvectors must lie in the subspace spanned by $\{(\lambda_i I - A)^{-1} B, i = 1, \dots, \max(m, q)\}$

where λ_i is the i^{th} closed-loop eigenvalues of the closed-loop system, $G \in \mathbb{R}^{m \times m}$ is the input weighting matrix of the closed-loop system, and $r(k)$ is the external input to the closed-loop system.

As stated in chapter 2, multiple-hypothesis Kalman filter and interacting multiple-model estimator can provide the overall probability-weighted state estimates, which makes it possible to apply the eigenstructure assignment by state feedback for the impaired system to maintain the overall system stability, and then to recover the performance as much of nominal system as possible.

3.3.1 Dynamic performance recovery-feedback controller design

Assignment of achievable eigenstructure For the nominal system with the state feedback K designed by LQR method:

$$x(k+1) = Ax(k) + Bu(k) \quad (3.3.3)$$

$$z(k+1) = Hx(k+1) \quad (3.3.4)$$

$$u(k) = Kx(k) \quad (3.3.5)$$

and the eigenstructure of closed-loop system is:

$$(A + BK)v_i = \lambda_i v_i \quad i = 1, \dots, n \quad (3.3.6)$$

Suppose that the dynamics of the system have undergone some changes due to faults in one or combination of system components, actuators, and sensors, and thus the system state-space description has vary from (A, B, H, K) to (A_f, B_f, H_f, K_f) , where “ f ” stands for failure. The system has become:

$$x(k+1) = A_f x(k) + B_f u(k) \quad (3.3.7)$$

$$z(k+1) = H_f x(k+1) \quad (3.3.8)$$

$$u(k) = K_f x(k) \quad (3.3.9)$$

with eigenstructure described as:

$$(A_f + B_f K_f)v_i^f = \lambda_i^f v_i^f \quad i = 1, \dots, n \quad (3.3.10)$$

As we know, eigenvalues determine the decay/growth rate of the system dynamic response, and the associated eigenvectors determine the shape of the response. The re-configured system can capture as much of the eigenstructure information characterizing the nominal closed-loop system as possible on the basis of the new feedback gain matrix K_f . Without loss of generality, we assume that the nominal closed-loop eigenvalues are arranged in decreasing order with respect to their real parts, that is $\Re(\lambda_1) \geq \Re(\lambda_2) \geq \dots \geq \Re(\lambda_n)$. It has been shown that all n closed-loop eigenvalues can be assigned with at most r entries of any one eigenvector. In order to maintain the performance of the nominal closed-loop system, a new feedback gain matrix K_f should be designed so that the closed-loop eigenvalues of the impaired system are the same as those of the nominal system. On the other hand, the associated eigenvectors of the reconfigured system have to be as close to the corresponding ones of the nominal closed-loop system as possible. The aim of reconfigurable control system design is translated into:

$$\lambda_i^f = \lambda(A_f + B_f K_f) = \lambda_i = \lambda(A + BK) \quad (3.3.11)$$

and

$$\min J_i(v_i^f) = \min[\|v_i - v_i^f\|^2] \quad i = 1, \dots, n \quad (3.3.12)$$

By rewriting (3.3.6), (3.3.10), the reconfigured system eigenvectors and nominal system eigenvectors will satisfy:

$$v_i^f = (\lambda_i^f I - A_f)^{-1} B_f K_f v_i^f \quad i = 1, \dots, n \quad (3.3.13)$$

$$v_i = (\lambda_i I - A)^{-1} B K v_i \quad i = 1, \dots, n \quad (3.3.14)$$

Note that the eigenvector of nominal system, v_i , is the desired eigenvector of v_i^f with the feedback gain matrix K_f . The above inverse $(\lambda_i^f I - A_f)^{-1}$ and $(\lambda_i I - A)^{-1}$ exist under the assumption that the closed-loop eigenvalues do not belong to the set of the open-loop eigenvalues, and the eigenvectors, v_i^f and v_i must be in the subspaces spanned by the columns of $(\lambda_i^f I - A_f)^{-1} B_f$ and by the columns of $(\lambda_i I - A)^{-1} B$ respectively. These subspaces are of the dimensions which are equal to the rank of B_f and the rank of B respectively which are equal to the number of independent control variables. Therefore, the number of control variables available determines how large (dimension) the subspace is in which achievable eigenvectors must reside. The orientation of the reconfigured system subspace is determined by the open-loop parameters described by A_f , B_f and the desired closed-loop eigenvalue λ_i^f , and the orientation of the nominal system subspace is by the open-loop parameters A , B and the closed-loop eigenvalue λ_i . In general, due to the variations in system dynamics, v_i^f does not lie in the same subspace as v_i . Instead of exactly recovering the v_i^f , a “best possible” choice for v_i^f is made. The best possible eigenvector, v_{i_A} , can be interpreted as the projection of desired eigenvector v_i onto the subspace spanned by the columns of $(\lambda_i^f I - A_f)^{-1} B_f$ as in Figure 3.1. Analytically, we compute $v_{i_A}^f$ by defining

$$E_i = (\lambda_i^f I - A_f)^{-1} B_f \quad (3.3.15)$$

and a new vector w_i can be defined as:

$$w_i = K_f v_i^f \quad (3.3.16)$$

Thus, (3.3.13) can be rewritten as:

$$v_i^f = E_i w_i \quad (3.3.17)$$

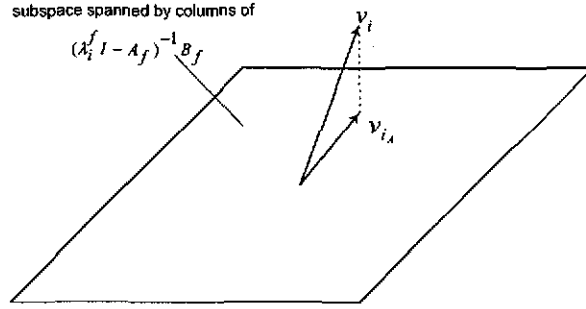


Figure 3.1: Geometric interpretation of v_i, v_{i_A}

To find the best possible eigenvector v_{i_A} is equivalent to find the vector w_i as a solution of least-square minimization problem (3.3.12), which can be rewritten as:

$$\min J_i(w_i) = \min(v_i - E_i w_i)^T W_i (v_i - E_i w_i) \quad (3.3.18)$$

where “ T ” stands for the transpose, and $W_i \in R^{n \times n}$ is a symmetric positive definite weighting matrix. The choice of the elements of W_i is pretty much problem dependent. In general, the larger the j^{th} diagonal element in W_i , the closer the j^{th} element in v_i^f to the corresponding elements in v_i . The solution of (3.3.18) is

$$w_i = (E_i^T W_i E_i)^{-1} E_i^T W_i^T v_i \quad (3.3.19)$$

$$v_i^f = E_i w_i \quad i = 1, \dots, n \quad (3.3.20)$$

By computing (3.3.11), (3.3.15), (3.3.19), we can get the achievable eigenstructures of the reconfigured system. The next step is to find the reconfigurable control gain matrix on the basis of the achievable eigenstructures.

Computation of reconfigurable control gain matrix The impaired system state-space equation (3.3.7) can be rewritten as

$$x(k+1) = (A_f + B_f K_f)x(k) \quad (3.3.21)$$

$$z(k+1) = H_f x(k+1) \quad (3.3.22)$$

In order to simplify the procedure in calculating the feedback gain matrix K_f , we consider the state-transformation defined by

$$x = T\tilde{x} \quad (3.3.23)$$

and select the transformation matrix

$$T = \left(B_f \mid S \right) \quad (3.3.24)$$

where $S \in \mathbb{R}^{n \times (n-m)}$ is any matrix such that $\text{rank}(T) = n$. Note that the choice of S is not unique. In this research, S is chosen as the $\text{null}(B_f)$ such that

$$S^T B_f = 0 \quad (3.3.25)$$

$$T^{-1} B_f = \begin{pmatrix} I \\ 0 \end{pmatrix} \quad (3.3.26)$$

By applying the above linear transformation, system equation (3.3.21) can be written as

$$\tilde{x}(k+1) = (\tilde{A}_f + \tilde{B}_f K_f T) \tilde{x}(k) \quad (3.3.27)$$

$$z(k+1) = \tilde{H}_f \tilde{x}(k+1) \quad (3.3.28)$$

where $\tilde{A}_f = T^{-1} A_f T$, $\tilde{B}_f = T^{-1} B$, and $\tilde{H}_f = H_f T$. and the corresponding eigenvectors under this linear transformation are related by

$$\tilde{v}_i^f = T^{-1} v_i^f \quad (3.3.29)$$

Each pair of achievable eigenvalues/eigenvector of the transformed system satisfies

$$(\lambda_i^f I - \tilde{A}_f) \tilde{v}_i^f = \tilde{B}_f K_f T \tilde{v}_i^f \quad (3.3.30)$$

By defining

$$\tilde{A}_f = \begin{pmatrix} \tilde{A}_{11} & \tilde{A}_{12} \\ \tilde{A}_{21} & \tilde{A}_{22} \end{pmatrix} \quad (3.3.31)$$

$$\tilde{v}_i^f = \begin{pmatrix} \tilde{f}_i \\ \tilde{l}_i \end{pmatrix} \quad (3.3.32)$$

where $\tilde{A}_{11} \in \mathfrak{R}^{m \times m}$, $\tilde{A}_{22} \in \mathfrak{R}^{(n-m) \times (n-m)}$, $\tilde{f}_i \in \mathfrak{R}^{m \times 1}$, and $\tilde{l}_i \in \mathfrak{R}^{(n-m) \times 1}$. In view of (3.3.25) and the above definitions, we can rewrite (3.3.30) as

$$\begin{pmatrix} \lambda_i^f I_{m \times m} - \tilde{A}_{11} & -\tilde{A}_{12} \\ -\tilde{A}_{21} & \lambda_i^f I_{(n-m) \times (n-m)} - \tilde{A}_{22} \end{pmatrix} \begin{pmatrix} \tilde{f}_i \\ \tilde{l}_i \end{pmatrix} = \begin{pmatrix} I_{m \times 1} \\ 0 \end{pmatrix} K_f T \tilde{v}_i^f \quad (3.3.33)$$

From (3.3.33), we can get

$$(\lambda_i^f I_{m \times m} - \tilde{A}_{11}) \tilde{f}_i - \tilde{A}_{12} \tilde{l}_i = K_f T \begin{pmatrix} \tilde{f}_i \\ \tilde{l}_i \end{pmatrix} \quad (3.3.34)$$

By defining

$$\tilde{A}_1 = \begin{pmatrix} \tilde{A}_{11} & \tilde{A}_{12} \end{pmatrix}, \quad (3.3.35)$$

(3.3.34) becomes

$$(\tilde{A}_1 + K_f T) \tilde{v}_i^f = \lambda_i^f \tilde{f}_i \quad i = 1, \dots, n \quad (3.3.36)$$

We can express (3.3.36) in a compact form

$$(\tilde{A}_1 + K_f T) \tilde{V} = \tilde{F} \quad (3.3.37)$$

where

$$\tilde{V} = \begin{pmatrix} \tilde{v}_1^f & \tilde{v}_2^f & \dots & \tilde{v}_n^f \end{pmatrix} \quad (3.3.38)$$

$$\tilde{F} = \begin{pmatrix} \lambda_1^f \tilde{f}_1 & \lambda_2^f \tilde{f}_2 & \dots & \lambda_n^f \tilde{f}_n \end{pmatrix} \quad (3.3.39)$$

If the achievable eigenvalues are all real, then the corresponding eigenvectors are real too, thus \tilde{V} and \tilde{F} are real, and the feed back gain matrix is

$$K_f = (\tilde{F} - \tilde{A}_1 \tilde{V})(T \tilde{V})^{-1} \quad (3.3.40)$$

However, when there is at least one pair of complex-conjugate eigenvalues/eigenvectors, both \tilde{V} and \tilde{F} are complex matrices. To alleviate the need for complex arithmetic, the following procedure is needed to transform them to real matrices.

Without loss of generality, we assume that $\lambda_1^f = (\lambda_2^f)^*$ and $\tilde{v}_1^f = (\tilde{v}_2^f)^*$, and all remaining eigenvalues/eigenvectors are real. Defining

$$\tilde{v}_1^f = \tilde{v}_1^R + j \tilde{v}_1^I \quad (3.3.41)$$

$$\lambda_1^f \tilde{f}_1 = \hat{f}_1^R + j \hat{f}_1^I \quad (3.3.42)$$

where \tilde{v}_1^R and \tilde{v}_1^I denote the real and imaginary parts of the eigenvector \tilde{v}_1^f respectively, and \hat{f}_1^R and \hat{f}_1^I are the real and imaginary parts of $\lambda_1^f \tilde{f}_1$. We rewrite (3.3.37) as

$$(\tilde{A}_1 + K_f T) \begin{pmatrix} \tilde{v}_1^R + j\tilde{v}_1^I & \tilde{v}_2^R - j\tilde{v}_2^I & \dots & \tilde{v}_n^f \end{pmatrix} = \begin{pmatrix} \hat{f}_1^R + j\hat{f}_1^I & \hat{f}_1^R - j\hat{f}_1^I & \dots & \lambda_n^f \tilde{f}_n \end{pmatrix} \quad (3.3.43)$$

Multiplying both sides of (3.3.43) with the nonsingular transformation matrix

$$\Lambda = \begin{pmatrix} 0.5 & -0.5j & 0 \\ 0.5 & 0.5j & 0 \\ 0 & 0 & I \end{pmatrix} \quad (3.3.44)$$

(3.3.43) becomes as

$$(\tilde{A}_1 + K_f T) \begin{pmatrix} \tilde{v}_1^R & \tilde{v}_1^I & \dots & \tilde{v}_n^f \end{pmatrix} = \begin{pmatrix} \hat{f}_1^R & \hat{f}_1^I & \dots & \lambda_n^f \tilde{f}_n \end{pmatrix} \quad (3.3.45)$$

$$(\tilde{A}_1 + K_f T)\hat{V} = \hat{F} \quad (3.3.46)$$

where

$$\hat{V} = \begin{pmatrix} \tilde{v}_1^R & \tilde{v}_1^I & \dots & \tilde{v}_n^f \end{pmatrix} \quad (3.3.47)$$

$$\hat{F} = \begin{pmatrix} \hat{f}_1^R & \hat{f}_1^I & \dots & \lambda_n^f \tilde{f}_n \end{pmatrix} \quad (3.3.48)$$

Thus the feedback gain matrix for the complex eigenvalues can be computed as

$$K_f = (\hat{F} - \tilde{A}_1 \hat{V})(T \hat{V})^{-1} \quad (3.3.49)$$

The generalization to the case of more complex conjugate pairs is straightforward.

3.3.2 Steady-state performance-recovery feedforward controller design

The dynamic performance of reconfigured system can be maintained to the maximum extent by exactly recovering the eigenvalues and achieving the best possible corresponding eigenvectors. It is very important to take into account the steady-state performance. This can be accomplished by a set of designed feedforward control gain matrices, G_j , $j = 1, \dots, M$, matching the corresponding system status. These feedforward gain matrices can be calculated using a property of z -transform.

For the system (3.3.7) with external input $r(k)$ weighted by feedforward gain matrix G_f , the state feedback law is

$$x(k+1) = (A_f + B_f K_f)x(k) + G_f r(k) \quad (3.3.50)$$

$$z(k+1) = H_f x(k+1) \quad (3.3.51)$$

The steady-state output of the stable closed-loop nominal system subject to a unit step input can be calculated using the final value theorem in z -transform

$$z(\infty) = \{\lim_{z \rightarrow 1} H_c(zI - A - BK)^{-1}B\}G = \{\lim_{z \rightarrow 1} H_c V \text{diag}\{\frac{1}{z - \lambda_i}\}V^{-1}\}G \quad (3.3.52)$$

where K represents the nominal system state feedback control gain, H_c is the matrix such that the system output $z(k) = H_c x(k)$ tracks the reference input $r(k)$. $\{\lambda_i, i = 1, \dots, n\}$ and $V = \begin{pmatrix} v_1 & v_2 & \dots & v_n \end{pmatrix}$ are the closed-loop eigenvalues, and eigenvector matrix.

Similarly, the steady-state output of the reconfigured system subject to a unit step input is

$$z(\infty) = \{\lim_{z \rightarrow 1} H_c(zI - A_f - B_f K_f)^{-1}B_f\}G_f = \{\lim_{z \rightarrow 1} H_c V_f \text{diag}\{\frac{1}{z - \lambda_i^f}\}V_f^{-1}\}G_f \quad (3.3.53)$$

where K_f represents the reconfigured system state feedback control gain. H_c is the matrix such that the system output $z(k) = H_c x(k)$ tracks the reference input $r(k)$. $\{\lambda_i^f, i = 1, \dots, n\}$ and $V = \begin{pmatrix} v_1^f & v_2^f & \dots & v_n^f \end{pmatrix}$ are the closed-loop eigenvalues and eigenvector matrix. By defining

$$\Psi = \{\lim_{z \rightarrow 1} H_c V \text{diag}\{\frac{1}{z - \lambda_i}\}V^{-1}\}G \quad (3.3.54)$$

$$\Phi = \{\lim_{z \rightarrow 1} H_c V_f \text{diag}\{\frac{1}{z - \lambda_i^f}\}V_f^{-1}\} \quad (3.3.55)$$

In view of above definition, the problem of maintaining the steady-state output performance with respect to unit step external input is to determine the appropriate G_f to minimize $J(G_f)$

$$\min J(G_f) = \min \|\Psi - \Phi G_f\|_F \quad (3.3.56)$$

The optimal solution is given by [8]

$$G_f = \Phi^+ \Psi \quad (3.3.57)$$

where $\Phi^+ = (\Phi^T \Phi)^{-1} \Phi^T$. It should be noted that the feedforward control gain G_f is dependent on the feedback control gain matrix K_f .

Table 3.3: Reconfigurable control signal generation scheme

$$\begin{array}{l} \text{if } \mu_j(k) < \mu_T \quad j = 1, \dots, n \\ \quad u(k) = \sum_{j=1}^M \mu_j(k) \{G_j r(k) + K_j \hat{x}_j(k)\} \\ \text{otherwise} \\ \quad u(k) = G_j r(k) + K_j \hat{x}_j(k) \quad j = \arg \max_i \mu_i(k) \end{array}$$

3.3.3 Reconfigurable control signal generation

On the basis of computations of the model-conditional probabilities and the pre-computed feedforward and feedback control gain matrices, the overall control signal into the plant can be generated by two ways: one is based on a Bayesian scheme and the other is by the maximum posterior probability (MAP) approach.

For the Bayesian approach, the control signal is obtained as the overall probability-weighted control signals from all models, which can be calculated as

$$u(k) = \sum_{j=1}^M \mu_j(k) \{G_j r(k) + K_j \hat{x}_j(k)\} \quad (3.3.58)$$

The advantage of this approach is that it is able to reduce the effect of incorrect model selection during the early stage of reconfiguration.

In the MAP approach, the control signal is chosen from the model with the highest probability.

$$u(k) = G_j r(k) + K_j \hat{x}_j(k) \quad j = \arg \max_i \mu_i(k) \quad (3.3.59)$$

Clearly, it is advantageous to combine those two approaches. If there is no failure, the Bayesian approach is used. Once the failure has been detected and identified, the control signal from the model with the highest probability will be used. The reconfigured control signal generation rules is described in Table 3.3.

Chapter 4

Simulation results

4.1 System state-space equation description

In this chapter, multiple-hypothesis Kalman filter based and IMM based FDI schemes are applied for the failure detection and identification of DC motor and VTOL aircraft model.

4.1.1 DC motor

Different measurable signals can be used to evaluate the response of the DC motor that is applied to control the motion of the aircraft flap. Measurable signals can be the angular position and velocity of the motor shaft, voltage and current at the terminal of the motors. For simplicity, we measure the angular position and velocity of the shaft, and the sensors used are gyroscope and incremental encoder [19].

Gyroscope The gyroscope measurement can be modelled as:

$$\omega_g = \omega + b + v_g \quad (4.1.1)$$

where ω is the true angular velocity of the shaft, v_g is additive white Gaussian noise with zero mean and certain covariance, and b is gyroscope bias drift term which is modeled as random walk:

$$\frac{db}{dt} = n_b \quad (4.1.2)$$

where n_b is assumed to be zero-mean Gaussian with known variance. The gyroscope measurement is assumed to be available at the Kalman Filter update rate, $T_g = 0.005$ seconds.

Incremental Encoder The incremental encoder can be modeled as:

$$\theta_e = \theta + v_e \quad (4.1.3)$$

where θ is the true angular position of the motor shaft and v_e is assumed to be zero-mean Gaussian with known variance. The encoder measurement is updated at the rate, $T_e = 0.05$ seconds.

Dc Motor Model The dynamics of a DC servo motor are described by the electrical signals and the mechanical motion of the armature as follows:

$$L_a \frac{di_a}{dt} + R_a i_a = v_a - K_e \dot{\theta} \quad (4.1.4)$$

$$J\ddot{\theta} + b\dot{\theta} = K_t i_a \quad (4.1.5)$$

where the symbols are listed in Table 4.1.

Table 4.1: DC motor model parameters

Symbol	Description
J	Moment of inertia of motor and load
b	Viscous damping of motor and load
L_a	Inductance of the armature
R_a	Resistance of the armature
v_a	Voltage across the terminal
K_e	Back EMF
K_t	Torque sensitivity
N	Gear Raio

Integrated Model Combining (4.1.1), (4.1.2), (4.1.3), (4.1.4), and (4.1.5), a continuous state-space model can be formulated as

$$\dot{x} = A_c x + B_c u + G_c n_b \quad (4.1.6)$$

Table 4.2: System Parameters description

$$\begin{aligned}
 A &= e^{A_c T_g} \simeq I + A_c T_g + \frac{(A_c T_g)^2}{2!} \\
 B &= \left(\int_0^{T_g} e^{A_c \tau} d\tau \right) B_c \simeq B_c T_g + \frac{A_c B_c T_g^2}{2!} \\
 Q &= \int_0^{T_g} e^{A_c(T-\tau)} G_c Q_c G_c^T e^{A_c^T(T\tau)} d\tau \simeq G_c Q_c G_c^T T_g + \frac{(A_c G_c Q_c G_c^T + G_c Q_c G_c^T A_c^T) T_g^2}{2!} \\
 R &= \begin{pmatrix} \frac{R_c}{T_e} & \frac{R_g}{T_g} \end{pmatrix}^T \\
 H &= \begin{cases} \begin{pmatrix} 1 & 0 & 0 & 0 \\ 0 & 1 & 0 & 1 \\ 0 & 1 & 0 & 1 \end{pmatrix} & t = t_{obs} \\ \begin{pmatrix} 0 & 0 & 0 & 0 \\ 0 & 0 & 0 & 0 \\ 0 & 0 & 0 & 0 \end{pmatrix} & \text{otherwise} \end{cases}
 \end{aligned}$$

where $x = \begin{pmatrix} \theta \\ \omega \\ i \\ b \end{pmatrix}$, $B_c = \begin{pmatrix} 0 & 0 \\ 0 & -\frac{N}{J} \\ \frac{1}{L_a} & 0 \\ 0 & 0 \end{pmatrix}$, $G_c = \begin{pmatrix} 0 \\ 0 \\ 0 \\ 1 \end{pmatrix}$, $u = \begin{pmatrix} v_a \\ T_L \end{pmatrix}$, and $A_c = \begin{pmatrix} 0 & \frac{1}{N} & 0 & 0 \\ 0 & -\frac{b}{J} & \frac{N^2 K_t}{J} & 0 \\ 0 & -\frac{K_e}{L_a} & -\frac{R_a}{L_a} & 0 \\ 0 & 0 & 0 & 0 \end{pmatrix}$.

The corresponding output equation is

$$z(t) = \begin{pmatrix} 1 & 0 & 0 & 0 \\ 0 & 1 & 0 & 1 \end{pmatrix} \begin{pmatrix} \theta \\ \omega \\ i \\ b \end{pmatrix} + \begin{pmatrix} v_e \\ v_g \end{pmatrix}$$

The discretization of (4.1.6) are described as

$$x(k+1) = Ax(k) + Bu(k) + w(k) \quad (4.1.7)$$

$$z(k+1) = Hx(k+1) + v(k+1) \quad (4.1.8)$$

where system parameters are described in Table 4.2. The specifications of Gyroscope and incremental encoder are listed in Table 4.3.

A simple diagram for the above state space representation is shown in Figure 4.1.

Table 4.3: Gyroscope and incremental encoder specification

Processing noise covariances:

$$\text{bias noise} = 3.0462\text{e-}006 \left(\frac{\text{rad}^2}{\text{sec}}\right)$$

Measurement noise covariances:

$$\text{gyro noise} = 1.1517\text{e-}009\left(\frac{\text{rad}}{\text{sec}}\right); \text{encoder noise} = 3\text{e-}10(\text{rad})$$

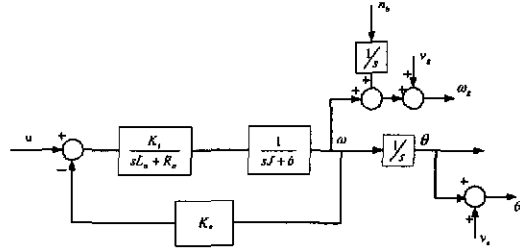


Figure 4.1: System model

4.1.2 VTOL aircraft model

The linear model for the aircraft can be described by

$$\dot{x}(t) = A_c x(t) + B_c u(t) + w(t) \quad (4.1.9)$$

$$z(t) = C_c x(t) + v(t) \quad (4.1.10)$$

where $x = (V_h \ V_v \ q \ \theta)^T$, $u = (\delta_c \ \delta_l)^T$. The states and inputs are: horizontal velocity V_h , vertical velocity V_v , pitch rate q , and pitch angle θ ; collective pitch control δ_c , and longitudinal cyclic pitch control δ_l . The subscript “c” stands for continuous. The model parameters are given as

$$A_c = \begin{pmatrix} -0.0366 & 0.0271 & 0.0188 & -0.4555 \\ 0.0482 & -1.01 & 0.0024 & -4.0208 \\ 0.1002 & 0.3681 & -0.707 & 1.420 \\ 0.0 & 0.0 & 1.0 & 0.0 \end{pmatrix}$$

$$B_c = \begin{pmatrix} 0.4422 & 0.1761 \\ 3.5446 & -7.5922 \\ -5.52 & 4.49 \\ 0.0 & 0.0 \end{pmatrix}, C_c = \begin{pmatrix} 1 & 0 & 0 & 0 \\ 0 & 1 & 0 & 0 \\ 0 & 0 & 1 & 0 \\ 0 & 1 & 1 & 1 \end{pmatrix}$$

The discretization of (4.1.9) can be represented by

$$x(k+1) = Ax(k) + Bu(k) + w(k) \quad (4.1.11)$$

$$z(k+1) = Hx(k+1) + v(k+1) \quad (4.1.12)$$

where $A = e^{AcT}$, $B = (\int_0^T e^{Ac\tau} d\tau)B_c$, and $H = C_c$, and the sampling period is $T = 0.1$ seconds. Processing noise covariances and measurement noise covariances are given as following: $Q = \text{diag}\{0.001^2, 0.001^2, 0.001^2, 0.001^2\}$, $R = \text{diag}\{0.01^2, 0.01^2, 0.01^2, 0.01^2\}$.

4.2 FDI performance evaluation of MH-KF and IMM algorithms

4.2.1 DC motor case

Figure 4.2 depicts an example of the failure scenario used for FDI performance evaluation.

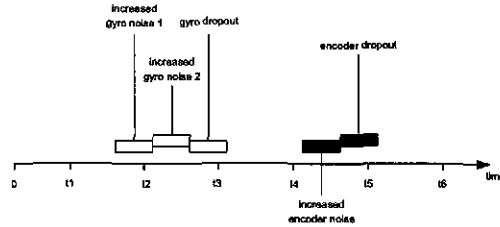


Figure 4.2: Time Sequence

The description of each possible operation mode of the integrated DC motor is explained in detail below.

- H0 *Nominal operation* – All systems are functioning properly. The nominal parameters used for the Kalman filter are representative of the actual system. Noise figures of the gyroscopes and encoders are directly taken from the sensor specifications.
- H1 *Noisy Gyro 1* – All the systems except the gyroscope are functioning properly. Partial failure of the gyroscope is simulated as the increase in the strength of the gyroscope measurement noise. The covariance of the noise of the gyroscope is increased by 50 times larger than the nominal value.
- H2 *Noisy Gyro 2* – Similar scenario as H1 but the strength of the gyroscope measurement noise is increased by 100 times larger than the nominal value.
- H3 *Failed Gyro* – All systems except the gyroscope are functioning properly. The gyroscope completely fails during service (Hard failure). It is not participating in measuring the response of the motor; it is only outputting signal composed of measurement noise.
- H4 *Noisy encoder* – All the systems except incremental encoder are functioning properly. Partial failure of the incremental encoder is modeled by increasing the covariance of the measurement noise of 100 times larger than the nominal value.
- H5 *Failed Encoder* – All the systems except the incremental encoder are functioning properly. Hard failure of the encoder is being expected. The output signal of the encoder is just the measurement noise.

Figure 4.3 depicts the sensor failures scenario. Because of the difference in the sampling rates between the gyroscope and incremental encoder, two parallel $MH - KF$ sets are used: $MH - KF^I$ considers gyroscope failures, while $MH - KF^{II}$ considers incremental encoder failures. $MH - KF^I$ uses the models: H0 nominal operation, H1 noisy gyro 1, H2 noisy gyro 2, and H3 failed gyro. $MH - KF^{II}$ uses the models: H0 nominal operation, H4 noisy encoder, and H5 failed encoder.

By choosing $N = 20$ as the “sliding window” size, the log-likelihood function values of $MH - KF^I$ are shown in Figure 4.4, and the log-likelihood function values of $MH - KF^{II}$ are shown in Figure 4.5. The mode which will be declared for the current

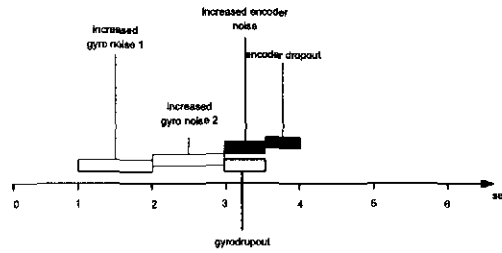


Figure 4.3: Failure sequence for DC motor

system operation mode is the corresponding filter with the maximum log-likelihood function value. In Figure 4.4, there is some incorrect fault identification in H2 period, and there is detection delay at the amount of NT_g for H3. In Figure 4.5, there are some incorrect fault identification in H5 period, and detection delay for H5.

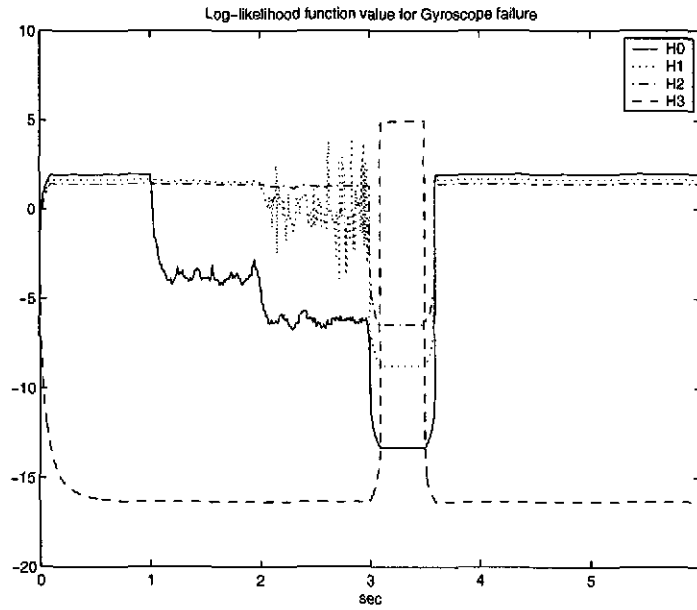


Figure 4.4: Log-likelihood function values of $MH - KF^I$ with $N = 20$

The incorrect fault identification can be reduced by increasing the “sliding window” size. As shown in Figure 4.6, and Figure 4.7, the window size N is equal to 40, and

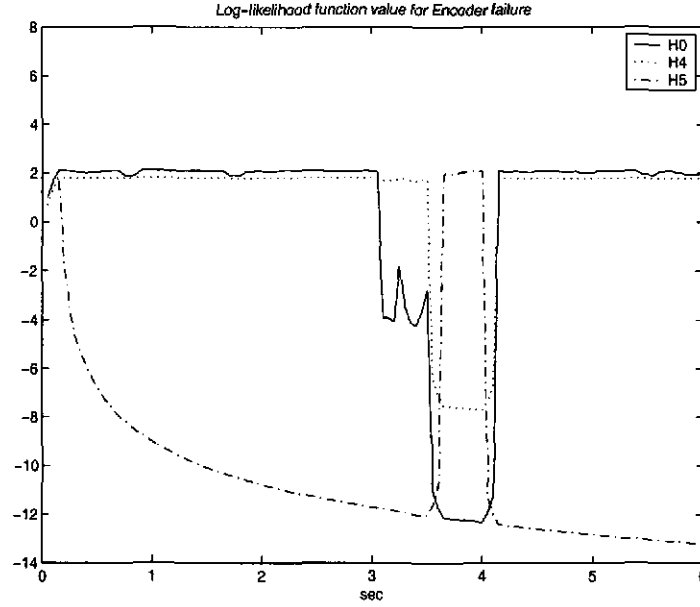


Figure 4.5: Log-likelihood function values of $MH - KF^{II}$ with $N = 20$

the incorrect fault identification occurrence is less than that of $N = 20$. Unfortunately, it will introduce more detection delay.

In general, all the failure modes can be detected by the comparison of the log-likelihood function value of each hypothesis under the certain fault tolerant. The detection delay can be shortening if the shorter sliding window is used. However, a small window size would increase the probability of incorrect fault identification.

As stated in chapter 3, we can compare the posterior or model-conditional probability of each system mode with the prespecified threshold p_T to make failure/no failure decision. Analysis of the mode-conditional probabilities for the $MH - KF^I$ and $MHKF^{II}$ clearly shows five failure periods in Figures 4.8 and 4.9. Posterior probabilities corresponding to the different hypothesis (H0, H1, H2, H3, H4, and H5) indicate when the gyro or incremental encoder is going to suffer the failures (represented by 0-1 and 1-0 switching). Furthermore, failures are identified unambiguously and almost instantaneously.

Assume that the gyroscope failures sequence and encoder failures sequence are first-order Markov chains with transition probability matrix H_g and H_e . Figure 4.10 and

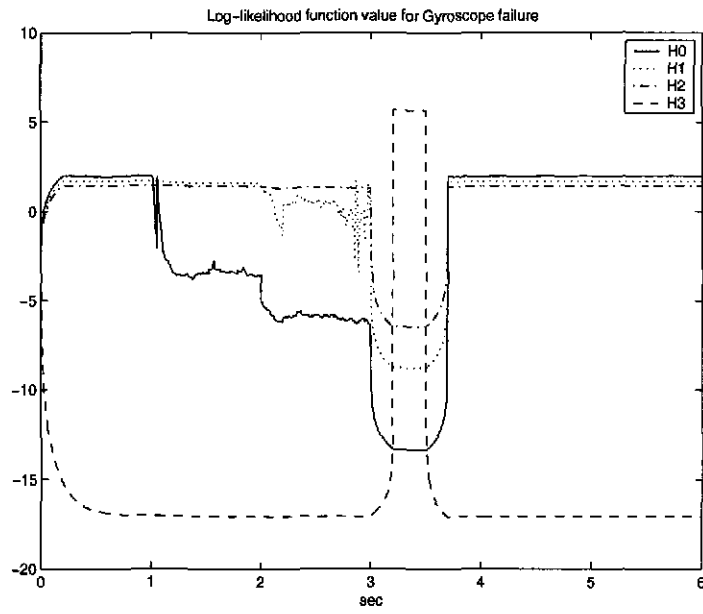


Figure 4.6: Log-likelihood function values of $MH - KF^I$ with $N = 40$

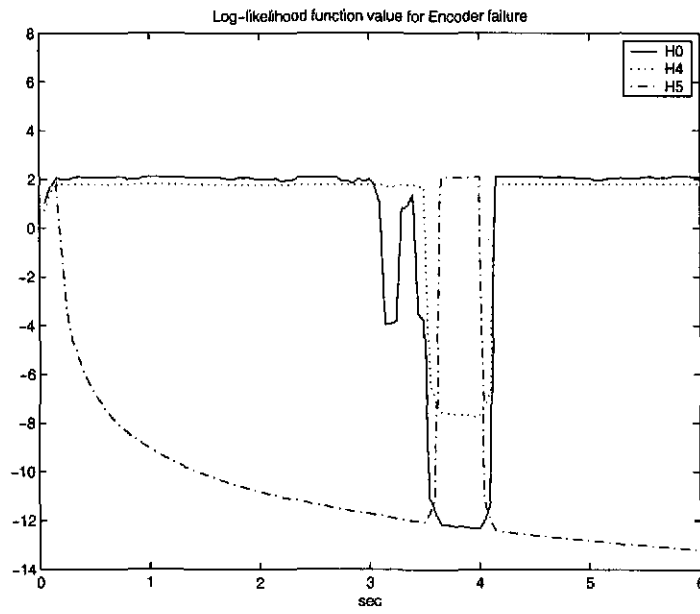


Figure 4.7: Log-likelihood function values of $MH - KF^{II}$ with $N = 40$

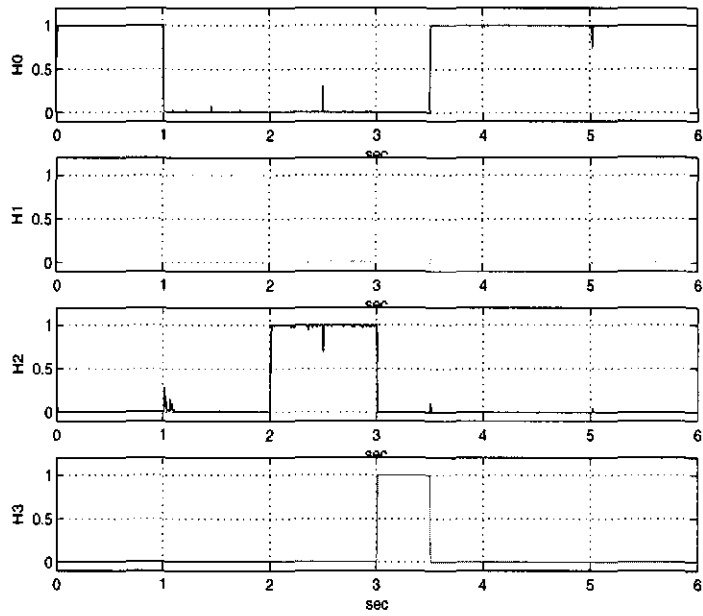


Figure 4.8: Posterior probabilities: $MH - KF^I$ with $MH - KF$ -based FDI scheme

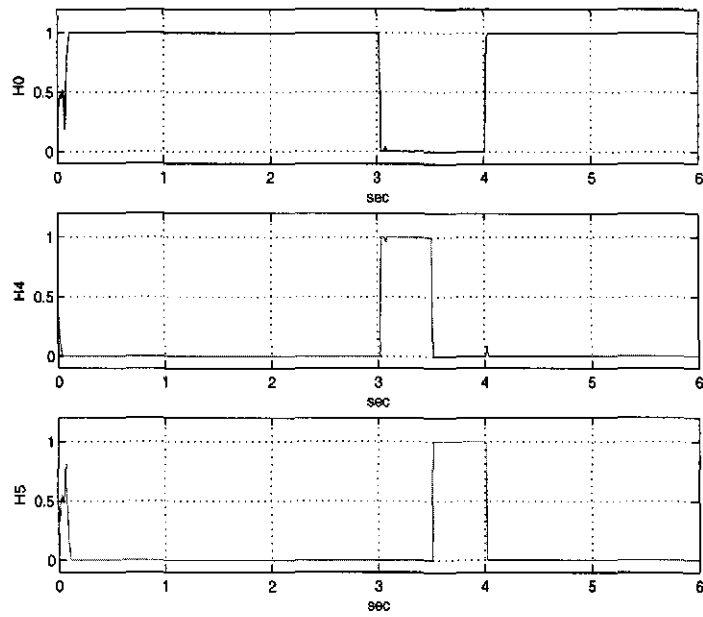


Figure 4.9: Posterior probabilities: $MH - KF^{II}$ with $MH - KF$ -based FDI scheme

Figure 4.11 depict the state transition diagram.

$$H_g = \begin{pmatrix} 0.97 & 0.01 & 0.01 & 0.01 \\ 0.02 & 0.98 & 0 & 0 \\ 0.02 & 0 & 0.98 & 0 \\ 0.02 & 0 & 0 & 0.98 \end{pmatrix}$$

and

$$H_e = \begin{pmatrix} 0.98 & 0.01 & 0.01 \\ 0.05 & 0.95 & 0 \\ 0.05 & 0 & 0.95 \end{pmatrix}$$

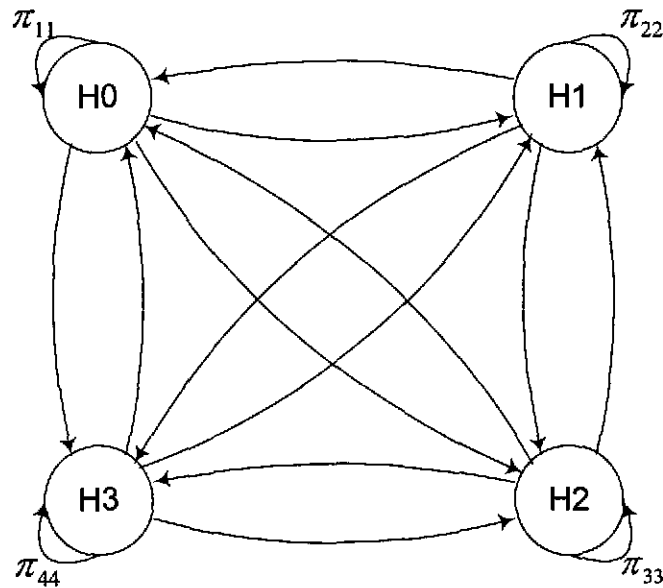


Figure 4.10: State transition diagram for $IMM - FDI^I$

The design strategies of transition probability matrix can be referred in [17]. Figure 4.12 and Figure 4.13 show the FDI simulation results using IMM-based FDI scheme. Here two parallel $IMM - FDI$ filters are used: $IMM - FDI^I$ considers gyroscope failure modes, while $IMM - FDI^{II}$ looks at encoder failure modes. $IMM - FDI^I$ includes H0, H1, H2, and H3, $IMM - FDI^{II}$ includes H0, H4, and H5. By looking at the

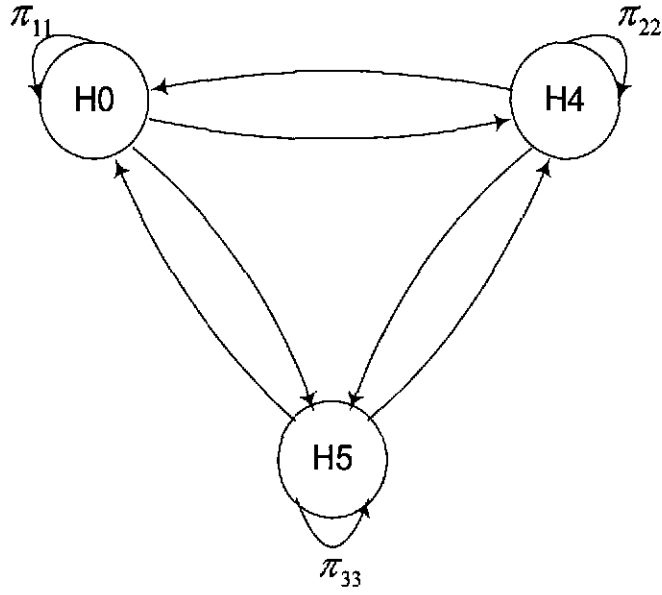


Figure 4.11: State transition diagram for $IMM - FDI^{II}$

switching of the model-conditional probability for each system mode, we can determine the system operation mode at any time, and detect the failures in operation and identify where the failure is.

For simulation results shown above, the shaft angular velocity and angular position estimation errors based on $MH - KF$ and IMM are compared in Figure 4.14. It can be noticed that estimation errors from IMM -based FDI scheme are consistently much less than that from $MH - KF$ based FDI scheme, and even below the measurement noise level. This just verifies that performance of IMM algorithm is superior to that of $MH - KF$ algorithm.

4.2.2 VTOL aircraft model case

The failure scenario of VTOL aircraft model is assumed in Figure 4.15. Referring to (4.1.7), we can calculate the eigenvalues of the open-loop system, $\Lambda = diag\{1.0276 + 0.0265i, 1.0276 - 0.0265i, 0.9770, 0.8142\}$. The unstable modes are $\lambda = 1.0276 \pm 0.0265i$. It is necessary to apply the state feedback to stabilize the system dynamic response. Here,

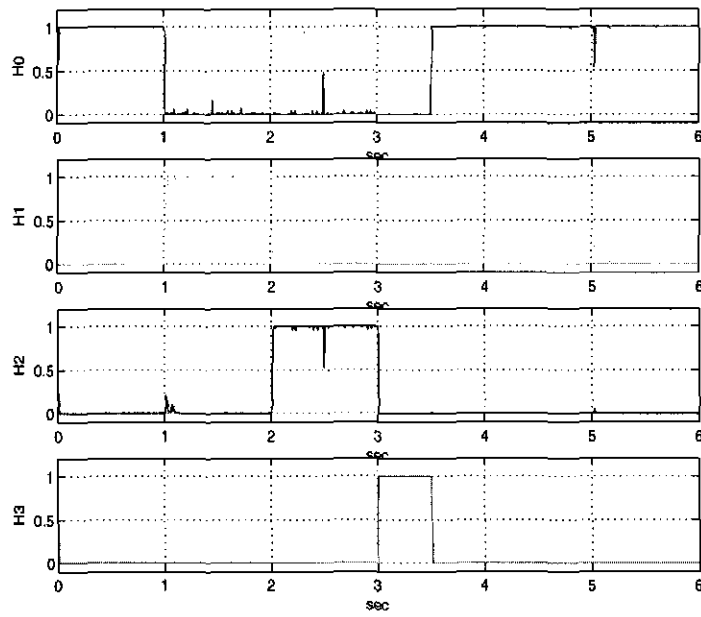


Figure 4.12: Posterior probabilities: $IMM - FDI^I$ with IMM -based FDI scheme

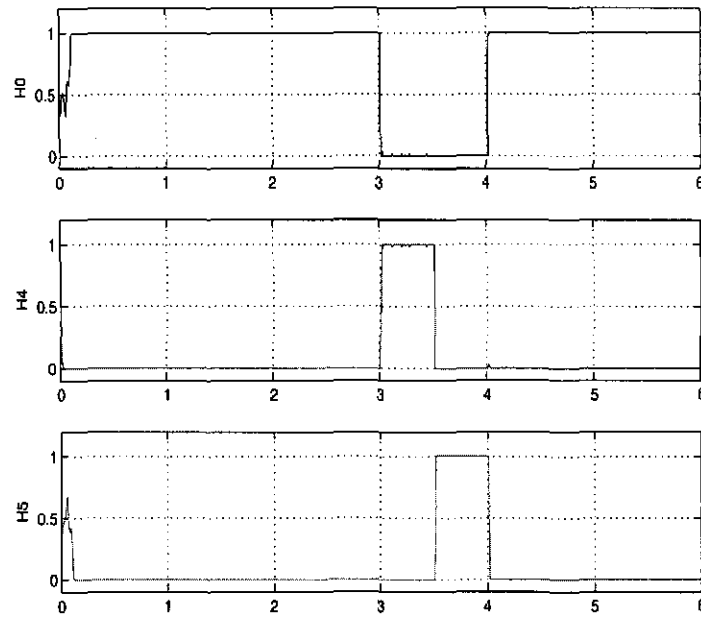


Figure 4.13: Posterior probabilities: $IMM - FDI^II$ with IMM -based FDI scheme

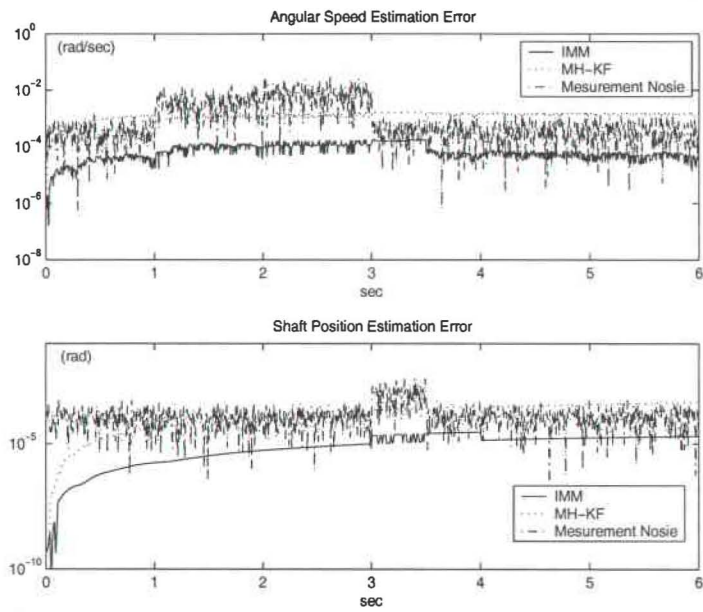


Figure 4.14: Estimation errors of Shaft angular velocity and angular position

LQR method is used to compute the feedback gain matrix K . Figure 4.16 depicts the system dynamic response after applied the state feedback. The initial conditions and other parameters are listed in Table 4.4.

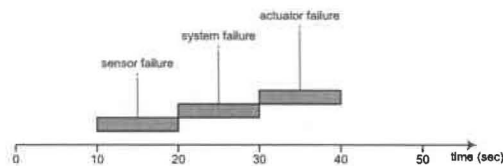


Figure 4.15: Failure scenario of VTOL aircraft model

The system possible modes are assumed to be H0 - nominal model, H1 - sensor failure, H2 - system failure, and H3 - actuator failure. System state-space description for each mode is referred as Table 4.5.

The “sliding window” size N is set to be equal to 10, and the log-likelihood function value for each system mode is in Figure 4.17. There exists false alarming and

Table 4.4: VTOL aircraft model design parameters

State and control weighting matrices:

$$Q_{LQR} = \text{diag}\{1, 1, 1, 1\} \text{ and } R_{LQR} = \text{diag}\{1, 1\}$$

State feedback gain matrix and feedforward control gain matrix:

$$K = \begin{pmatrix} 1.2551 & 0.2243 & -1.2954 & -1.9315 \\ -0.2728 & -1.2669 & 0.4872 & 1.1662 \end{pmatrix}, G = \begin{pmatrix} 1.3428 & 0.2573 \\ -0.2603 & -1.4540 \end{pmatrix}$$

Initial condition and the external control input:

$$x_0 = (25 \ 5 \ 1 \ 0.8)^T, \text{ and } r = (1 \ 1)^T$$

Initial conditions for each Kalman filter:

$$x_j^0 = (25 \ 5 \ 1 \ 0.8)^T$$

$$P_j^0 = \text{diag}\{0.001^2, 0.001^2, 0.001^2, 0.001^2\}$$

$$Q_j = \text{diag}\{0.001^2, 0.001^2, 0.001^2, 0.001^2\}, \text{ and } R_j = \text{diag}\{0.01^2, 0.01^2, 0.01^2, 0.01^2\}$$

The command tracking matrix H_c :

$$H_c = \begin{pmatrix} 1 & 0 & 0 & 0 \\ 0 & 1 & 0 & 0 \end{pmatrix}$$

Table 4.5: System matrices for nominal and fault modes

Modes	A_j	B_j	H_j
Fault-free ($j = 1$)	$\begin{pmatrix} 0.9964 & 0.0026 & -0.0005 & -0.0459 \\ 0.0046 & 0.9041 & -0.0199 & -0.3819 \\ 0.0097 & 0.0337 & 0.9389 & 0.1294 \\ 0.0005 & 0.0018 & 0.0965 & 1.0071 \end{pmatrix}$	$\begin{pmatrix} 0.0441 & 0.0170 \\ 0.3366 & -0.7208 \\ -0.5257 & 0.4192 \\ -0.0276 & 0.0225 \end{pmatrix}$	$\begin{pmatrix} 1 & 0 & 0 & 0 \\ 0 & 1 & 0 & 0 \\ 0 & 0 & 1 & 0 \\ 0 & 1 & 1 & 1 \end{pmatrix}$
Sensor fault ($j = 2$)	$\begin{pmatrix} 0.9964 & 0.0026 & -0.0005 & -0.0459 \\ 0.0046 & 0.9041 & -0.0199 & -0.3819 \\ 0.0097 & 0.0337 & 0.9389 & 0.1294 \\ 0.0005 & 0.0018 & 0.0965 & 1.0071 \end{pmatrix}$	$\begin{pmatrix} 0.0441 & 0.0170 \\ 0.3366 & -0.7208 \\ -0.5257 & 0.4192 \\ -0.0276 & 0.0225 \end{pmatrix}$	$\begin{pmatrix} 0 & 0 & 0 & 0 \\ 0 & 1 & 0 & 0 \\ 0 & 0 & 1 & 0 \\ 0 & 1 & 1 & 1 \end{pmatrix}$
System fault ($j = 3$)	$\begin{pmatrix} 0.9964 & 0.0026 & -0.0005 & -0.0459 \\ 0.0046 & 0.0 & -0.0199 & -0.3819 \\ 0.0097 & 0.0337 & 0.9389 & 0.1294 \\ 0.0005 & 0.0018 & 0.0965 & 1.0071 \end{pmatrix}$	$\begin{pmatrix} 0.0441 & 0.0170 \\ 0.3366 & -0.7208 \\ -0.5257 & 0.4192 \\ -0.0276 & 0.0225 \end{pmatrix}$	$\begin{pmatrix} 1 & 0 & 0 & 0 \\ 0 & 1 & 0 & 0 \\ 0 & 0 & 1 & 0 \\ 0 & 1 & 1 & 1 \end{pmatrix}$
Actuator fault ($j = 4$)	$\begin{pmatrix} 0.9964 & 0.0026 & -0.0005 & -0.0459 \\ 0.0046 & 0.9041 & -0.0199 & -0.3819 \\ 0.0097 & 0.0337 & 0.9389 & 0.1294 \\ 0.0005 & 0.0018 & 0.0965 & 1.0071 \end{pmatrix}$	$\begin{pmatrix} 0.0441 & 0.0170 \\ 0.0 & -0.7208 \\ -0.5257 & 0.0 \\ -0.0276 & 0.0112 \end{pmatrix}$	$\begin{pmatrix} 1 & 0 & 0 & 0 \\ 0 & 1 & 0 & 0 \\ 0 & 0 & 1 & 0 \\ 0 & 1 & 1 & 1 \end{pmatrix}$

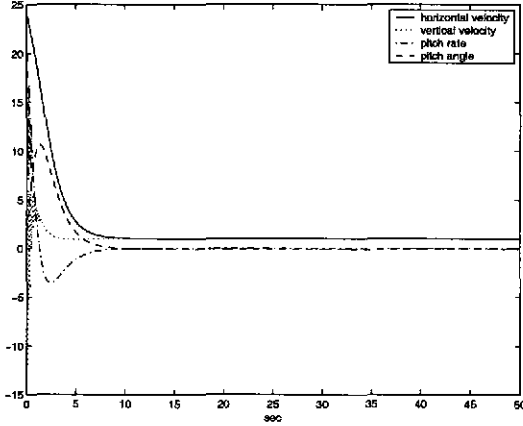


Figure 4.16: System dynamic response with state feedback

delay for fault detection and identification; also it is not convenient to make the failure/no failure decision by comparing log-likelihood function values.

The system mode sequence can be modeled as a four-state Markov chain with transition probability matrix H_T . The state transition can be illustrated as Figure 4.10. By using IMM-based FDI scheme, the simulation results without applying reconfigurable control system to the fault modes are shown in Figure 4.18. As we can see, IMM-based FDI algorithm can detect and identify the fault modes unambiguously and almost instantaneously.

$$H_T = \begin{pmatrix} 87/90 & 1/90 & 1/90 & 1/90 \\ 0.01 & 0.99 & 0 & 0 \\ 0.01 & 0 & 0.99 & 0 \\ 0.01 & 0 & 0 & 0.99 \end{pmatrix} \quad (4.2.1)$$

4.3 Performance evaluation of FTCS for VTOL aircraft model based on IMM

According to performance evaluation of two proposed FDI schemes, multiple-hypothesis Kaman filter and interacting multiple-model estimator, we can conclude that IMM-based FDI scheme can outperform the MH-KF-based FDI scheme on both state esti-

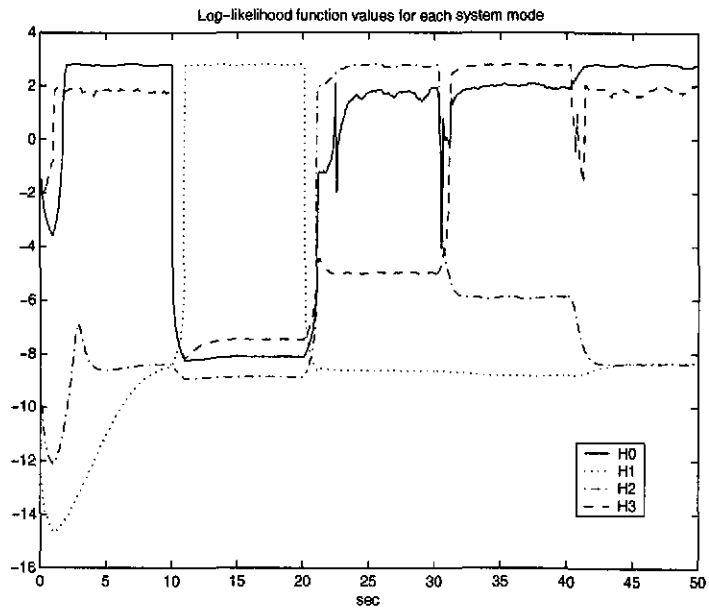


Figure 4.17: Log-likelihood function values for VTOL aircraft system modes with $N = 10$

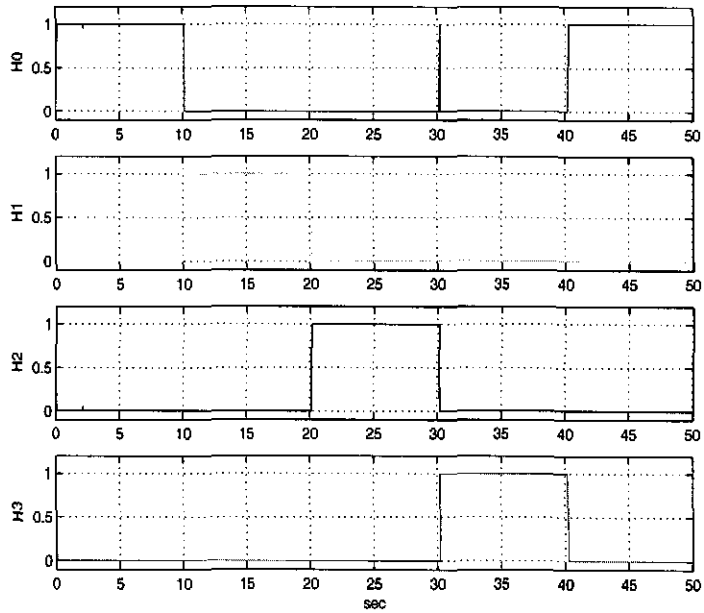


Figure 4.18: IMM-based FDI simulation for VTOL aircraft system modes

mation and failure detection and identification. Parameters in Table 4.4 are used to design the Kalman filters and reconfigurable control system. In addition to the conventional performance indices, such as false alarm (FA) and missed detection (MD), the following performance indices are designed and used in performance evaluation: average percentages of correct detection and identification (CDID), incorrect mode identification (IFID), no mode detection (NMD).

- 1) one CDID is counted if the model that is closest to the system mode (normal or fault mode) in effect at a given time has a probability higher than the threshold $\mu_T = 0.9$
- 2) one IFID is counted if the model with a probability over μ_T is not the one closest to the fault mode in effect at a given time
- 3) one FA is counted if the model with a probability over μ_T is not the normal mode while the normal mode is in effect at the given time
- 4) one MD is counted if the normal model has the highest probability which exceeds μ_T while the system has a fault
- 5) one NMD is counted if no model has a probability greater than μ_T

It is desirable to have higher CDID and lower FA, IFID, MD, and NMD.

4.3.1 Eigenstructure and reconfigurable control gain

The eigenvalues and eigenvectors of the closed-loop system in fault-free mode and different fault modes are presented in Table 4.6 and Table 4.7, respectively. The reconfigurable control gain matrices are shown in Table 4.8. It is clear that the eigenvalues of the fault modes can be exactly recovered and the corresponding eigenvectors can be assigned as close to those of the nominal system as possible. We can calculate the misalignment of the eigenvectors in terms of distance and angles between them to see how quantitatively close they are.

Assume that the failure scenario of VTOL aircraft model is shown as Figure 4.15, and the system-mode sequence is a four-state Markov chain with state transition probability H_T (4.2.1). The state response under reconfigurable control is illustrated in Figure 4.19

Table 4.6: Eigenvalues for nominal and fault modes

	Fault-free	Sensor fault	System fault	Actuator fault
Eigenvalues	$\begin{pmatrix} -0.7501 \\ 0.9254 \\ 0.8962 \\ 0.7708 \end{pmatrix}$	$\begin{pmatrix} -0.7501 \\ 0.9254 \\ 0.8962 \\ 0.7708 \end{pmatrix}$	$\begin{pmatrix} -0.7501 \\ 0.9254 \\ 0.8962 \\ 0.7708 \end{pmatrix}$	$\begin{pmatrix} -0.7501 \\ 0.9254 \\ 0.8962 \\ 0.7708 \end{pmatrix}$

Table 4.7: Eigenvectors of nominal and fault modes

Modes	Eigenvectors	Misalignment in distance/angle(rad)
Fault-free	$\begin{pmatrix} -0.0122 & -0.5995 & -0.4420 & 0.2244 \\ -0.7584 & 0.0456 & 0.1164 & -0.4785 \\ 0.6517 & 0.4910 & 0.6586 & -0.7927 \\ -0.0025 & -0.6304 & -0.5978 & 0.3039 \end{pmatrix}$	$\begin{pmatrix} 0 \angle 0 \\ 0 \angle 0 \\ 0 \angle 0 \\ 0 \angle 0 \end{pmatrix}^T$
Sensor fault	$\begin{pmatrix} -0.0122 & -0.5995 & -0.4420 & 0.2244 \\ -0.7584 & 0.0456 & 0.1164 & -0.4785 \\ 0.6517 & 0.4910 & 0.6586 & -0.7927 \\ -0.0025 & -0.6304 & -0.5978 & 0.3039 \end{pmatrix}$	$\begin{pmatrix} 0 \angle 0 \\ 0 \angle 0 \\ 0 \angle 0 \\ 0 \angle 0 \end{pmatrix}^T$
System fault	$\begin{pmatrix} -0.0563 & -0.5806 & 0.3870 & 0.0375 \\ -0.7615 & 0.0195 & -0.0639 & -0.4204 \\ 0.6457 & 0.5002 & -0.6814 & -0.8471 \\ -0.0029 & -0.6421 & 0.6179 & 0.3230 \end{pmatrix}$	$\begin{pmatrix} 0.0447 \angle 0.0447 \\ 0.0355 \angle 0.0355 \\ 1.9983 \angle 3.0605 \\ 0.2040 \angle 0.2044 \end{pmatrix}^T$
Actuator fault	$\begin{pmatrix} -0.0329 & -0.4483 & -0.3086 & 0.1271 \\ -0.7589 & 0.0574 & 0.1253 & -0.4846 \\ 0.6503 & 0.5225 & 0.6813 & -0.8045 \\ 0.0085 & -0.7230 & -0.6518 & 0.3189 \end{pmatrix}$	$\begin{pmatrix} 0.0235 \angle 0.0235 \\ 0.1804 \angle 0.1806 \\ 0.1460 \angle 0.1461 \\ 0.0994 \angle 0.0994 \end{pmatrix}^T$

Table 4.8: Controller gains for fault-free and reconfigured systems

Modes	Feedback control gains	Feedforward control gains
Fault-free	$\begin{pmatrix} 1.2551 & 0.2243 & -1.2954 & -1.9315 \\ -0.2728 & -1.2669 & 0.4872 & 1.1662 \end{pmatrix}$	$\begin{pmatrix} 1.3428 & 0.2573 \\ -0.2603 & -1.4540 \end{pmatrix}$
Sensor fault	$\begin{pmatrix} 1.2551 & 0.2243 & -1.2954 & -1.9315 \\ -0.2728 & -1.2669 & 0.4872 & 1.1662 \end{pmatrix}$	$\begin{pmatrix} 1.3428 & 0.2573 \\ -0.2603 & -1.4540 \end{pmatrix}$
System fault	$\begin{pmatrix} 1.2596 & 1.5712 & -1.4483 & -2.0145 \\ -0.4584 & 0.7518 & 0.5173 & 1.3997 \end{pmatrix}$	$\begin{pmatrix} 1.3492 & 3.4449 \\ -0.4513 & -2.5497 \end{pmatrix}$
Actuator fault	$\begin{pmatrix} 2.2964 & 1.1254 & -1.6745 & -2.7788 \\ -1.3557 & -1.3126 & 1.0865 & 2.0253 \end{pmatrix}$	$\begin{pmatrix} 2.4770 & 0.9808 \\ -1.4450 & -1.3224 \end{pmatrix}$

in the presence of sensor fault, system fault and actuator fault; as we can see, the sensor fault has no any effect on the state dynamic response, while the system fault and actuator failure do have. By applying IMM-based FTCS to the aircraft model, the mode probability transition is illustrated in Figure 4.20. It can be observed that there are a few mis-switching between the nominal mode and actuator fault mode, a few amount of detection delay for each fault mode. Overall, the fault mode has been correctly diagnosed. The quantitative performance indices are given in Table 4.9. The results in Table 4.9 are the average of 50 Monte Carlo simulation runs. Compared the performance indices values of reconfigured system with ideal values of the performance indices in Table 4.10, satisfactory FDI performance has been obtained via IMM-based FDI scheme.

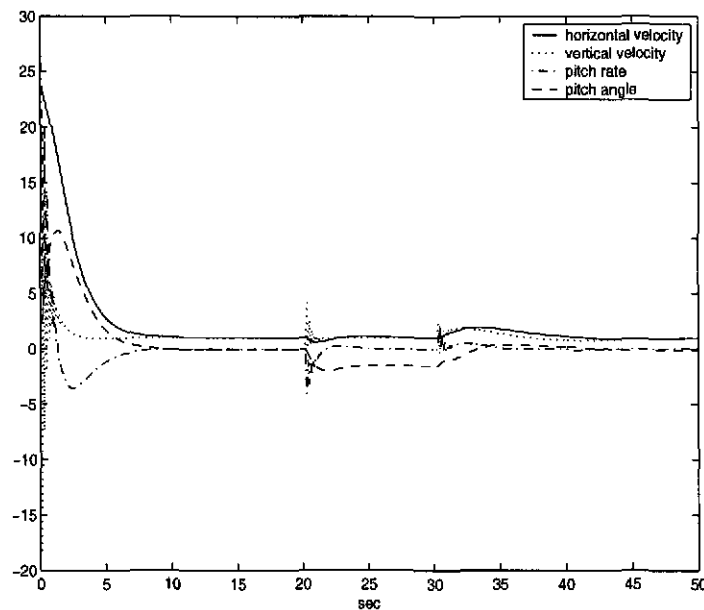


Figure 4.19: State response under reconfigurable control

Since the controlled variables are horizontal velocity and vertical velocity, it is necessary to see how the reconfigurable control system affect those two channels. The effects of reconfigurable control system on horizontal velocity and vertical velocity are illustrated in Figure 4.21, and Figure 4.22 respectively. Without reconfiguration, the output response will blow up, this is not allowed in many aircraft control system.

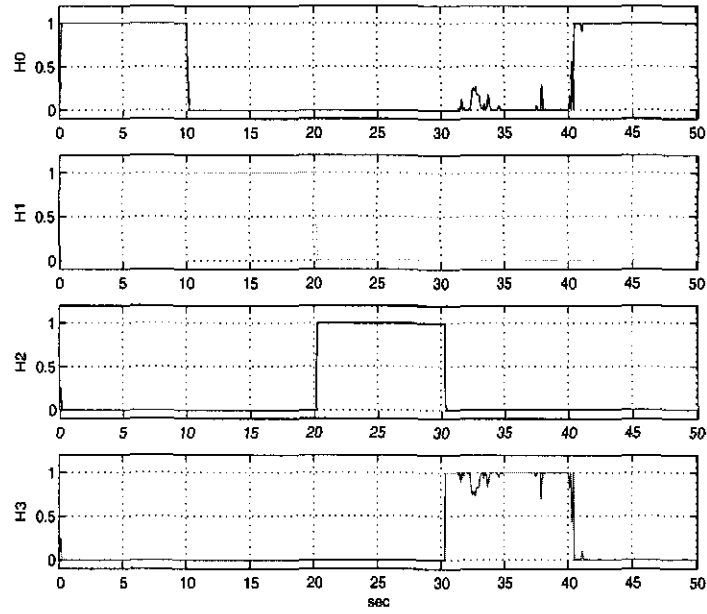


Figure 4.20: Mode transition probability under reconfigurable control

Table 4.9: Values of quantitative performance indices

Modes	CDID	IFID	FA	MD	NMD
Fault-free	98.48%	-	0.51%	-	3.6%
Sensor fault	99.01%	0.99%	-	0.99%	3.6%
System fault	99.01%	0.99%	-	0%	3.6%
Actuator fault	92.18%	0.99%	-	0%	3.6%

Table 4.10: Ideal values of quantitative performance indices

Modes	CDID	IFID	FA	MD	NMD
Fault-free	100%	-	0%	-	0%
Sensor fault	100%	0%	-	0%	0%
System fault	100%	0%	-	0%	0%
Actuator fault	100%	0%	-	0%	0%

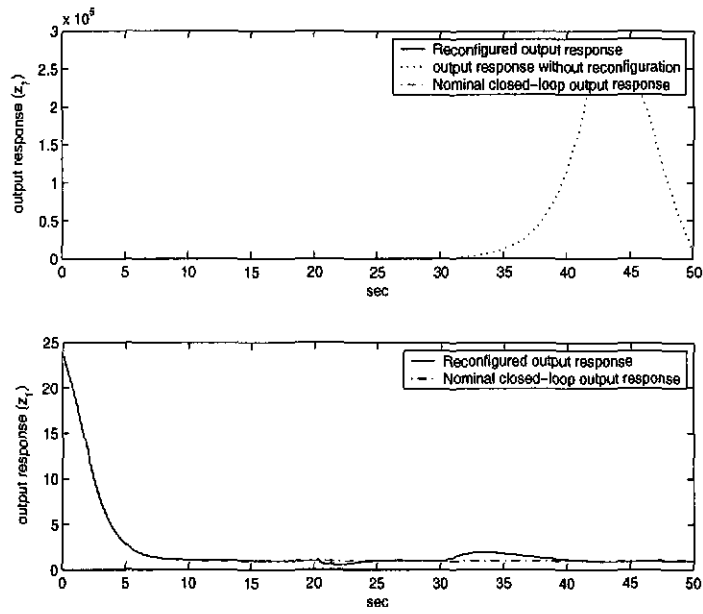


Figure 4.21: Output response z_1 under faults

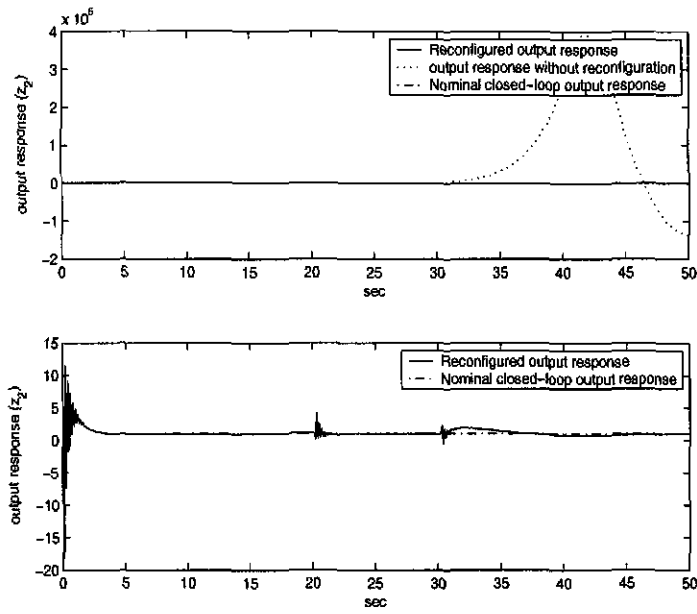


Figure 4.22: Output response z_2 under faults

The above performance evaluations of two proposed FDI approaches and IMM-based fault-tolerant control system have indicated that the multiple-hypothesis Kalman filter and interacting multiple-model estimator can detect and identify the failure correctly, and IMM-based FDI and reconfigurable control scheme can deal with system component, actuator and sensor failures effectively.

Chapter 5

Conclusion

5.1 Discussions

For the multiple-model based approaches, multi-hypothesis Kalman filter and interacting multiple model estimator, the actual system can be modeled as a stochastic hybrid system sufficiently and accurately, in which the status of the system at any time is determined among a set of possible operation modes according to the decision algorithms, such as Maximum log-likelihood function (MLLF), Bayesian scheme, and Maximum a Posterior Probability. The simulation presented in this thesis shows that the multiple-model based FDI approaches can detect and identify the complicated failure scenario very well under the certain fault tolerance. As we can see, the multi-hypothesis Kalman filter is very sensitive to the sliding window size used to calculate the log-likelihood function value. The way to choosing appropriate window size should be followed: the window size should be kept greater than one to prevent failure declarations due to a single residual sample of large magnitude, consistently large residuals indicate abnormalities, whereas individual realizations of large magnitude are to be expected, while it is inappropriate to use all the residuals from the initial time to current time, since this would decrease the sensitivity to true failures as time processed. Thus a "sliding window" of the N most recent samples, with N on the order of 5 to 20, would be suggested. The most of the detection delay is introduced by using the sliding window method. In order to avoid the shortcoming of MLLF, the model-conditional probability (MCP) is suggested for decision algorithm. The simulation result

shows that model-conditional probability algorithm outperforms MLLF. Neither MLFF nor MCP considers the interaction among the Kalman filters. With the assumption that the system modes can be modeled as a finite-state Markov chain, the interacting multiple-model estimator can dramatically improve the FDI performance and provide much better state estimation.

Linear quadratic regulator and eigenstructure assignment schemes are used to design the reconfigurable controller for nominal and fault system modes respectively. The IMM-based FDI scheme and reconfigurable controller design scheme are integrated to deal with the VTOL aircraft model suffered from the system component, actuator, and sensor failures. The simulation results and values of performance indices have shown the effectiveness of the integrated FDI and reconfigurable control scheme.

5.2 Future work

In this research, the possible system modes are prespecified; however, it is very crucial to design the set of possible system operation modes to match the real system operation status, especially for very complicated system and real-time FDI. In order to describe the system operation as accurately as possible, the vehicle's dynamic response and subsystem models need to be understood thoroughly, and it is applicable to couple the IMM-based FDI with neural network as shown in Figure 5.1. The neural network is going to train the system operation mode based on the input and output, and the new system mode information is added into the IMM filter bank, feedback controller bank and feedforward controller bank. Existing FDI algorithms will continually be intensively studied to improve the performance, reduce the computational complexity and cost of implementation.

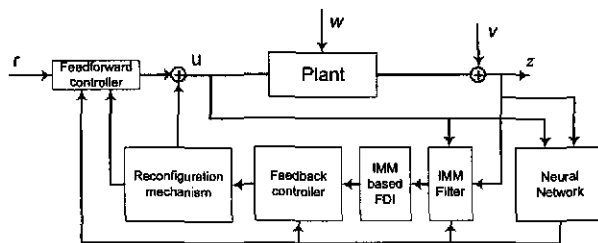


Figure 5.1: General structure of IMM-based FDI and reconfigurable control scheme with neural network

Bibliography

- [1] Ali Zolghadri, “*An algorithm for real time failure detection in kalman filters*”, IEEE Transactions on Automatic Control, Vol. 41, No. 10, 1996, pp.1537-1539.
- [2] Mehra, R., and Peschon, J., “*An innovation approach to fault detection and diagnosis in dynamic systems*”, Automatica, 7:637-640, Pergamon Press, 1971.
- [3] Willsky, A., “*A survey of design methods for failure detection*”, Automatica., Nov. 1976, pp. 601-611.
- [4] Kerr, T., “*Real-time failure detection: A static nonlinear optimization problem that yields a two ellipsoid overlap test*”, Journal of Optimization Theory and Applications, Vol. 22, August 1977.
- [5] Kerr, T., “*Statistical analysis of a two-ellipsoid overlap test for real-time failure detection*”, IEEE Transaction on Automatic Control, Vol. AC-25, No. 4 August 1980, pp.762-773.
- [6] Maybeck, P.S. “*Stochastic models, estimation, and control Volume 1*”, ACADEMIC PRESS, INC. 1979.
- [7] Andry, A. N., Shapiro, E. Y. JR., and Chung, J. C., “*Eigenstructure assignment for linear systems*”, IEEE Transaction on Aerospace and Electronic Systems, Vol. AES-19, No. 5, September 1983, pp.711-728
- [8] Golub, G. H., and Van Loan, C. F. “*Matrix Computations*”, The JONhs Hopkins University Press.

- [9] Blom, H. A., and Bar-Shalom, Y. "*The interacting multiple model algorithm for systems with Markovian switching coefficients*", IEEE Transaction on Automatic Control, Vol. 33, No. 8 August 1988, pp.780-783
- [10] Maybeck, P.S., and Stevens, R. D. "*Reconfigurable flight control via multiple model adaptive control methods*", IEEE Transactions on Aerospace and Electronic Systems, Vol 27, No. 3, 1991, pp. 470-479.
- [11] Jiang, J. "*Design of reconfigurable control system using eigenstructure assignment*", International Journal of Control, 59, 1994, pp.395-400.
- [12] Lewis, F. L., and Syrmos, V. L., "*Optimal Control*", JOHN WILEY & SONS, INC. 1995.
- [13] Maybeck, P.S., and Hanlon, R. D. "*Performance enhancement of a multiple model adaptive estimator*", IEEE Transactions on Aerospace and Electronic Systems, Vol 31, No. 4, 1995, pp. 1240-1254.
- [14] Menke, T.E., and Maybeck, P.S. "*Sensor/actuator failure detection in the Vista F-16 by multiple model adaptive estimation*", IEEE Transactions on Aerospace and Electronic Systems, Vol 31, No. 4, 1995, pp. 1218-1229.
- [15] Li, X. R., and BarShalom, Y., "*Multiple-model estimation with variable structure*", IEEE Transactions on Automatic Control, 41, 4, 1996, pp. 393-406.
- [16] R. Mehra, C. Rago, and S. Seereeram, "*Autonomous failure detection, identification and fault-tolerant estimation with aerospace application*", IEEE Aerospace Conference Proceeding, Vol. 2, 1998, pp. 134-138.
- [17] Zhang, Y. M., and Li, X. R., "*Detection and diagnosis of sensor and actuator failures using IMM estimator*", IEEE Transactions on Aerospace and Electronic Systems, Vol 34, No. 4, 1998, pp. 1293-1313.
- [18] Hanlon, P. D., and Maybeck, P. S., "*Multiple-Model Adaptive Estimation using a residual correlation kalman filter bank*", IEEE Transactions on Aerospace and Electronic Systems, Vol 36, No. 2, 2000, pp. 393-406.

- [19] Syrmos Vassilis, "*Vehicle health monitoring system failure detection and identification*", Technical report, 2002.